Analytical Methods

ROYAL SOCIETY OF CHEMISTRY

CRITICAL REVIEW

View Article Online
View Journal | View Issue

Cite this: *Anal. Methods*, 2025, **17**, 6264

Carbon-based nanozymes: catalytic mechanisms, performance tuning, and environmental and biomedical applications

Hongying Ye, Yongquan Lai, Zhaodi Wu, Guizhen Li, Qingqing Hua and Wenyuan Zhu *

Carbon-based nanozymes—a significant subclass of nanomaterials mimicking natural enzyme catalytic functions—offer superior thermal/chemical stability and enhanced biocompatibility compared to natural enzymes and other nanozyme types, owing to their unique carbon matrix. This review comprehensively examines research progress in carbon-based nanozymes. It details their classification into three categories: (1) carbon nanozymes (*e.g.*, fullerenes, graphene, carbon dots, and nanotubes), (2) heteroatom-doped variants (N, P, S, and Se), and (3) metal/metal oxide-supported types, including single-atom nanozymes with M–N_x–C sites. The primary catalytic mechanisms, focusing on peroxidase (POD)-like and superoxide dismutase (SOD)-like activities, alongside oxidase (OXD)-like and catalase (CAT)-like mechanisms, are discussed. Strategies for regulating nanozyme performance—such as size/morphology control, composition/structure tuning (doping and defect engineering), surface modification, biomolecular interactions, and external environment manipulation (pH and temperature)—are highlighted. The review emphasizes the broad applications of carbon-based nanozymes in environmental engineering (pollutant detection/degradation), biosensing (H_2O_2, biomolecules, antioxidants, and tumor markers), and biomedicine (antioxidant/anti-inflammatory therapy, tumor treatment, antibacterial/antiviral applications, and bioimaging). Finally, it addresses existing challenges, including relatively lower activity/specificity compared to natural enzymes, limited enzyme-mimicking types, unclear atomic-scale mechanisms, synthesis control difficulties, biocompatibility/safety concerns, and the need for standardized research frameworks. This overview underscores the immense potential and future research directions for carbon-based nanozymes.

Received 15th June 2025
Accepted 14th July 2025

DOI: 10.1039/d5ay00997a

rsc.li/methods

1. Introduction

Natural enzymes, which are proteins or RNA with high specificity and catalytic efficiency produced by living cells,[1] are widely used in industrial and biomedical fields.[2–5] Although natural enzymes play irreplaceable roles in various fields owing to their biological catalytic functions, they exhibit inevitable limitations.[6,7] For instance, they are easily inactivated under non-physiological conditions,[6] thus irreversibly losing their catalytic activity. In addition, the extraction and purification processes of natural enzymes are complex, time-consuming and costly.[6] These inherent drawbacks significantly hinder the practical applications of natural enzymes. In order to avoid the above-mentioned limitations and broaden the application fields, researchers have successively proposed substitutes with catalytic activity comparable to that of natural enzymes—nanozymes.

Guangxi Key Laboratory of Electrochemical and Magneto-Chemical Functional Materials, College of Chemistry and Bioengineering, Guilin University of Technology, Guilin 541006, P. R. China. E-mail: wyzhu@glut.edu.cn

Nanozymes are a novel class of nanomaterials with catalytic functions[8] combining the unique properties of nanomaterials with the catalytic characteristics of natural enzymes.[9] They are now widely used in biosensing,[9,10] disease treatment,[11,12] and environmental engineering.[8] Since the discovery of Fe_3O_4 nanoparticles exhibiting peroxidase (POD)-like activity in 2007,[13] various nanomaterials with enzyme-mimicking properties, including metals, metal oxides, carbon-based nanomaterials, and metal–organic frameworks (MOFs),[14] have been developed. These materials achieve efficient catalysis through surface effects and size effects, among other mechanisms. Compared to natural enzymes, nanozymes exhibit superior stability and are less affected by harsh conditions such as high temperatures and extreme pH.[9] Furthermore, their preparation is typically simple and cost-effective,[15] facilitating large-scale production.

Carbon-based nanozymes are a new class of synthetic nanomaterials[16] and a significant category within nanomaterial research. They hold unique advantages in the field, being primarily composed of carbon-based materials, including fullerenes, graphene,[17] carbon nanotubes, carbon quantum

dots, and graphene quantum dots.[14,18] Through specific designs and techniques, these materials can imitate the catalytic functions of natural enzymes.

Generally speaking, carbon-based nanozymes exhibit the following characteristics:[18] first, they provide abundant active sites,[7] thereby enabling efficient catalysis of various reactions to meet diverse catalytic needs. Furthermore, compared with natural enzymes, they exhibit better thermal and chemical stability and can maintain stable catalytic activity even in harsh environments.[7] Additionally, carbon-based nanozymes demonstrate good biocompatibility[19] and biosafety,[12] implying low risks and side effects in biomedical applications. Notably, their catalytic activity can be regulated by methods, such as chemical modification and doping,[20] optimizing the performance and specificity to meet different application requirements. Moreover, their manufacturing costs are relatively low, aligning with sustainability principles. Specifically, carbon materials are abundant, environmentally friendly, and low-cost, fitting well with sustainable development principles. Last but not least, carbon-based nanozymes often possess catalytic properties along with additional functionalities such as conductivity and adsorption.

This article provides a comprehensive overview of carbon-based nanozymes, including their classification, diverse catalytic mechanisms, and performance regulation strategies. Furthermore, research on their applications in multiple domains will be discussed in detail, and the existing challenges will be summarized.

2. Categorization of carbon-based nanozymes

Carbon, a fundamental component of all living things on Earth, can form stable covalent bonds with various atoms to construct complex structures. So far, a variety of carbon-based nanozymes have been developed. Based on composition and structural characteristics, they are primarily classified into three categories: carbon nanozymes, heteroatom-doped carbon-based nanozymes, and metal/metal oxide-supported carbon-based nanozymes.[21] The synthesis of these carbon-based nanozymes not only reflects the structural diversity of carbon-based materials but also fosters in-depth research into the catalytic

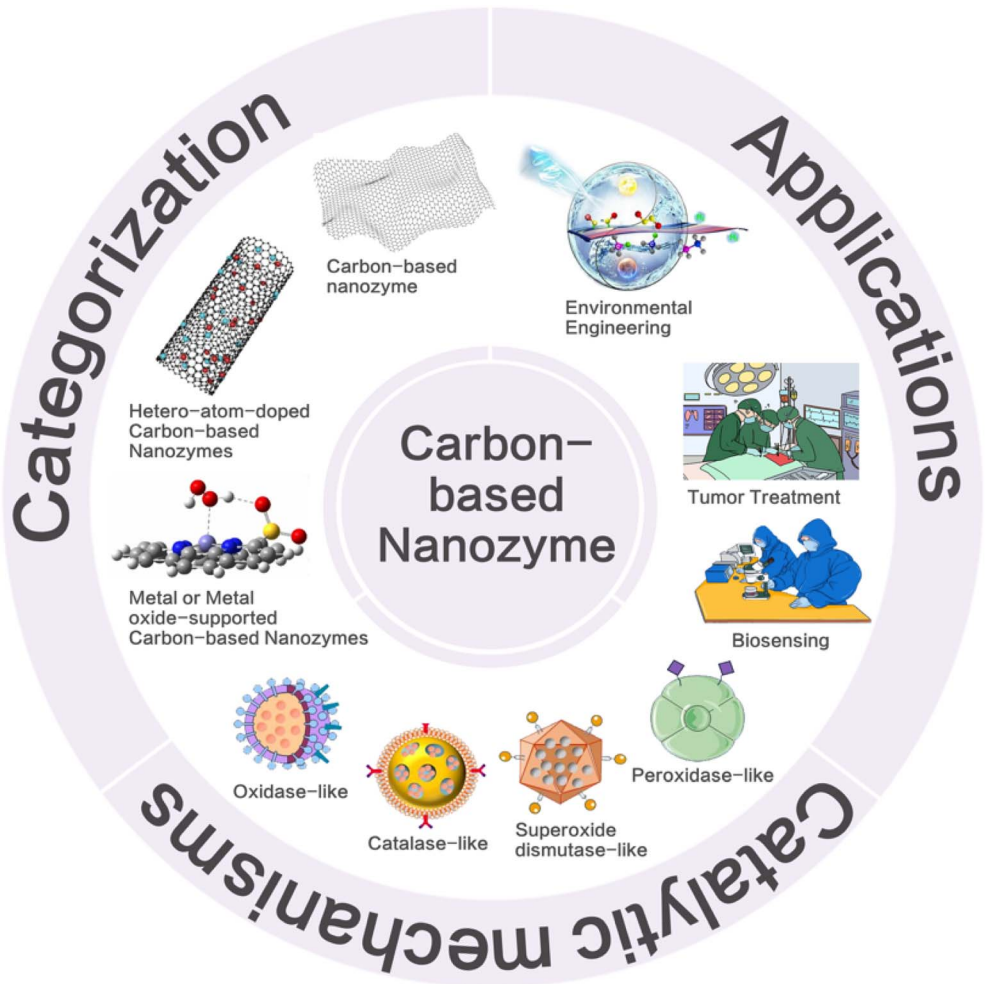

Fig. 1 Classification of carbon-based nanozymes: (a) fullerene nanozymes, (b) graphene nanozymes, (c) carbon nanotube nanozymes, and (d) carbon dot nanozymes.

mechanisms of carbon-based materials and their application potential in various fields.

2.1. Carbon-based nanozymes

Carbon nanozymes can be traced back to 1996 when Dugan *et al.*[22] discovered that fullerene derivatives possess superoxide dismutase-like activity and can scavenge superoxide anion radicals. Since then, research has been conducted on carbon-based materials, including fullerenes, graphene,[17] carbon dots, carbon nanotubes, carbon nanospheres and carbon nanofibers.[23] Their enzyme-like activities have increasingly been studied,[14] often focusing on the construction of their derivatives.

Among these carbon nanozymes:

• Fullerene nanozymes often exhibit nuclease-like activity and possess rich chemical composition, small size, and uniform dispersibility. However, their closed structure limits the overall number of active sites, resulting in relatively low catalytic activity.

• Graphene nanozymes exhibit excellent peroxidase (POD)-like activity. For instance, Huang *et al.*[17] prepared POD-active graphene-based materials using hydrothermal reduction with *Ganoderma lucidum* polysaccharides. Carboxylated graphene oxide (GO–COOH) exhibits stronger affinity for organic TMB due to the π–π conjugation effect.[24]

• Carbon nanotube nanozymes (Fig. 1c) like their carbon dot counterparts exhibit enhanced peroxidase (POD)-like activity when modified with functional groups. For example, Wang *et al.*[25] synthesized oxidized carbon nanotubes (o-CNTs) using green methods (Fig. 2),[25] confirming their POD-like activity with abundant surface oxygen-containing functional groups identified as the catalytic active sites.

• Carbon dot nanozymes commonly bear abundant hydrophilic functional groups (*e.g.*, carbonyl, carboxyl, and hydroxyl[25]) on their surfaces. These groups provide numerous active sites for interacting with substrates, thereby enhancing the catalytic efficiency. Additionally, they confer high water solubility and ease of functionalization. Leveraging these characteristics, carbon dot nanozymes and related carbon nanomaterials show broad application prospects in biomedicine, clinical diagnosis, and biocatalysis.

• Carbon nanosphere nanozymes can demonstrate various enzyme-like activities through elemental doping, while their closed structure helps minimize interference from oxygen defects.

• Carbon nanofiber nanozymes are a class of artificial enzyme-mimicking materials based on carbon nanofibers. Their catalytic activity and selectivity can be modulated through strategies such as doping (*e.g.*, with nitrogen or boron) or surface functionalization (*e.g.*, by introducing metal nanoparticles). Research has shown that defective sites and edge carbon atoms on the surface of carbon nanofibers can catalyze the decomposition of hydrogen peroxide to generate reactive oxygen species (ROS). This property enables their application in areas like tumor therapy and pollutant degradation.[26]

Collectively, these studies provide valuable insights for the rational design of carbon-based nanozymes and their derivatives. However, for pure carbon materials, their inherent rigid structure may result in relatively low activity or insufficient substrate recognition. In addition, these carbon-based nanozymes incorporate responsive carbon-based materials, which can undergo controllable structural or property changes in response to external stimuli such as light, heat, pH, electric fields, or magnetic fields. Crucially, the electron distribution within these carbon materials can be modulated through heteroatom doping (*e.g.*, N and S). This modulation is particularly effective in enhancing their responsiveness to specific stimuli like light and electric fields. Therefore, constructing enzyme-like active sites through element doping presents a promising strategy to enhance their activity, specificity and application fields.

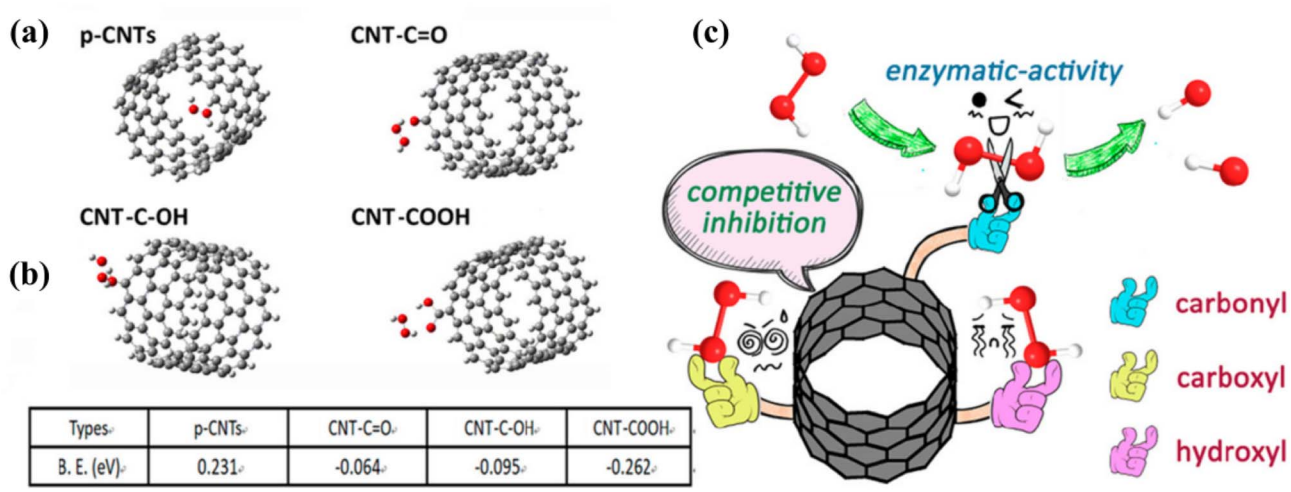

Types	p-CNTs	CNT-C=O	CNT-C-OH	CNT-COOH
B. E. (eV)	0.231	-0.064	-0.095	-0.262

Fig. 2 (a) Optimized binding modes and (b) binding energies (Δ*G*) of H_2O_2 in functionalized CNT surfaces: CNT=O, CNT–C–OH, and CNT–COOH; (c) schematic of the peroxidase (POD)-like catalytic mechanism in oxidized CNTs (o-CNTs).

2.2. Hetero-atom-doped carbon-based nanozymes

Carbon-based nanozymes regulate their specificity and catalytic activity by introducing heteroatoms into carbon materials. These heteroatoms, such as nitrogen (N), phosphorus (P), sulfur (S), and selenium (Se), alter the electronic structure and surface properties of materials like carbon dots, graphene, and carbon nanotubes. Single heteroatom doping is the most fundamental strategy to modulate the electronic structure of carbon-based nanozymes. By precisely controlling the type, number and position of the dopant atoms, the electronic distribution and energy band structure of carbon materials can be targeted to modulate their enzyme-like catalytic activity. Among the many dopant elements, nitrogen (N) is the most widely studied, primarily due to its similar atomic radius to carbon and unique electron-donating properties. The nitrogen atom (five valence electrons) replaces a carbon atom (four valence electrons) in the lattice, contributing an additional electron to the π-conjugated system.[27] This shifts the Fermi energy level upward and increases the electron density,[28] endowing nitrogen-doped carbon materials with enhanced electron-donating capacity[29] that facilitates electron transfer in catalysis.

Beyond nitrogen, other non-metallic heteroatoms exhibit distinct modulation effects. For example, boron (B) doping introduces electron holes due to its three valence electrons[30]—one less than carbon. Consequently, this electron-deficient state enables p-type semiconductor properties, allowing attraction of electrons from oxygen or H_2O_2 to facilitate their decomposition. Sulfur (S) and phosphorus (P) doping introduce more complex electronic effects.[31,32] Their larger atomic radii (*vs.* carbon) induce localized strains and lattice defects that alter the charge distribution. Sulfur-doped materials specifically show excellent redox activity,[32] attributed to sulfur-induced spin density redistribution and charge polarization.

In conclusion, heteroatom-doped carbon-based nanozymes demonstrate superior selectivity in mimicking natural enzymes compared to undoped analogues, showing significant research and application potential.

The synthesis of these nanozymes employs diverse methods, including hydrothermal treatment, chemical vapor deposition (CVD), and solution-based approaches. For example, nitrogen-doped carbon dots (N-CDs), nitrogen/sulfur-doped carbon dots (N,S-CDs), and sulfur-doped reduced graphene oxide (S-rGO)[20] can be synthesized hydrothermally. Wu *et al.*[20] prepared sulfur-

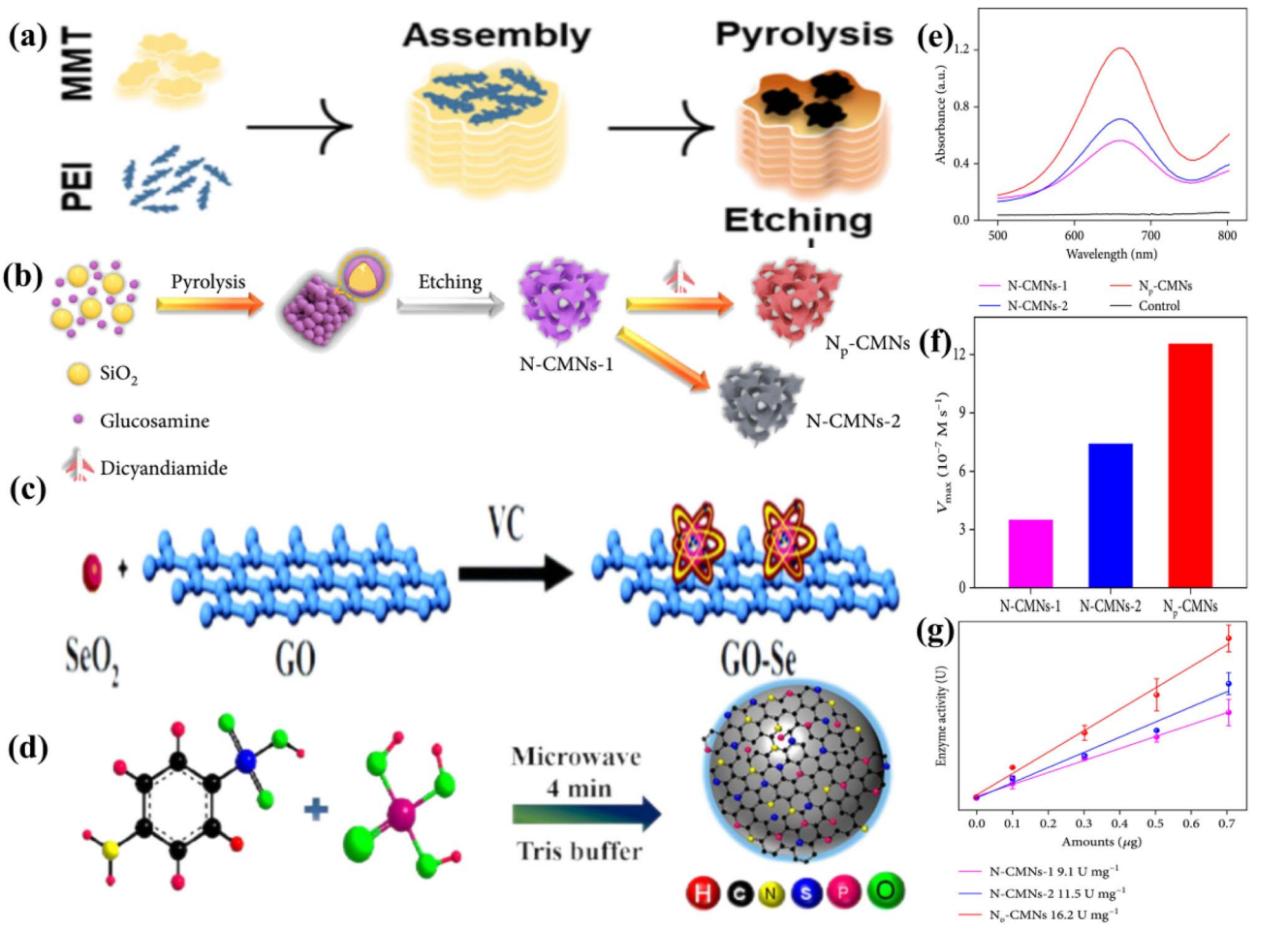

Fig. 3 Synthesis of (a) N-doped carbon sheets *via* strong electrostatic attraction between MMT and PEI, (b) N-CMNs, (c) GO–Se nanocomposites, and (d) NSP-CQDs. (e) UV-vis absorption spectra of POD-like catalytic oxidation with N-CMNs. (f) V_{max} (H_2O_2 substrate) and (g) specific activity (SA) of N-CMNs.

doped graphene oxide (S-GO) *via* a simple hydrothermal reaction, eliminating the need for templates and surfactants. Compared to its undoped precursor, this material showed significantly enhanced peroxidase (POD)-like activity, indicating that sulfur-containing groups serve as major active sites. The chemical vapor deposition (CVD) method produces large-area, high-quality graphene and carbon nanotubes. Solution-based methods are straightforward and scalable. Lou *et al.*[33] synthesized a highly N-doped carbon nanozyme (Fig. 3a), with XPS analysis revealing four nitrogen configurations: pyridinic N, graphitic N, pyrrolic N, and oxidized N. Yan *et al.*[34] employed secondary N-doping to fabricate porous carbon nanozymes with a tunable pyridinic-N content, exhibiting peroxidase-like activity (Fig. 3b). Their study demonstrated a positive correlation between the pyridinic-N content and peroxidase (POD)-like activity (Fig. 3e–g). In contrast, Gu *et al.*[35] reported distinct catalytic roles for nitrogen species in iron-coordinated systems: pyrrolic-N coordinates Fe(III) as the dominant active site, while pyridinic-N coordinates Fe(II) with minimal activity contribution. The low D-band center position at pyrrolic-N–Fe sites facilitates Fe–oxo intermediate formation, enhancing the catalytic performance.

Beyond nitrogen doping, non-metallic sites (*e.g.*, Se) in graphene confer enzyme-mimicking activities. For example, GO–Se nanozymes (Fig. 3c) exhibit glutathione peroxidase (GP_x)-like activity.[36] Co-doping synergistically enhances activity *versus* single-heteroatom doping. Chen *et al.*[37] achieved N,S-co-doped porous carbon nanozymes showing 3.9-fold higher specific activity and 11.8-fold greater H_2O_2 affinity than N-doped analogs, enabling TAC detection in beverages *via* POD-like activity. Kim *et al.*[38] synthesized N,B-co-doped rGO (NB-rGO), exhibiting 40-fold and 35-fold higher catalytic activity toward TMB and H_2O_2, respectively, *versus* undoped rGO. DFT calculations revealed N,B co-doping activates pyridinic-N, with boron serving as a co-active site. Tripathi *et al.*[39] developed N,P,S-co-doped CQDs (Fig. 3d), where multi-heteroatom synergy enhanced the catalytic activity and broadened the operational pH range.

2.3. Metal- or metal oxide-supported carbon-based nanozymes

Metal/metal oxide doping into carbon-based nanozymes addresses the easy aggregation and high cost of pure metal nanozymes. Additionally, metal-carbon synergies further enhance the catalytic activity and stability. Gao *et al.*[40] immobilized Fe_3O_4 nanoparticles on aminopyridine-functionalized multi-walled carbon nanotubes (MWCNT-AP), obtaining well-dispersed superparamagnetic Fe_3O_4/MWCNT-AP nanocomposites. The enhanced POD-like activity enables phenolic compound degradation in environmental waters. Similarly, *in situ* anchoring of copper nanoparticles onto aminated graphene quantum dot frameworks modulate enzyme-like activity and enhances H_2O_2 affinity. At 7.66% loading, Cu single-atom nanozymes (SAN) exhibited 3.4-fold higher POD activity and 8.88-fold greater SOD activity than low-loading counterparts,[41] demonstrating loading-dependent selectivity. Xie *et al.*[42] prepared ultrathin Cu/CN nanosheets (Fig. 4a) *via* supramolecular pre-organization/calcination, achieving 14.3 wt% Cu loading. High-density atomic Cu sites confer exceptional peroxidase (POD)-like activity.

Researchers have discovered single-atom nanozymes (SAzymes) with M–N_x–C sites resembling natural metalloenzyme centers, where M is a transition metal (Fe, Co, Pt, Mn, and Cu). These SAzymes mimic the homogeneous active centers of natural enzymes, exhibiting ultrahigh atomic utilization efficiency and tunable coordination environments.[43] Under optimized conditions, they demonstrate catalytic activities and reaction kinetics comparable to natural enzymes.[44] During high-temperature pyrolysis, metal precursors enable direct synthesis of SAzymes *via* strong interactions with pyrolytic intermediates. Consequently, numerous studies employed pyrolytic synthesis (Fig. 4a–d). Wu *et al.*[45] used ZIF-8 to disperse atomic Fe uniformly in N-doped carbon matrices. Subsequent carbonization/activation (Fig. 4b) yielded 2D ultrathin Fe–N–C SAzymes with high surface area and hierarchical porosity. Jiao *et al.*[46] developed atomic-scale SAzymes using salt templating (Fig. 4c), achieving 13.5 wt% Fe loading in N-doped carbon nanosheets. Zn (Co)–N–C SAzymes prepared similarly showed

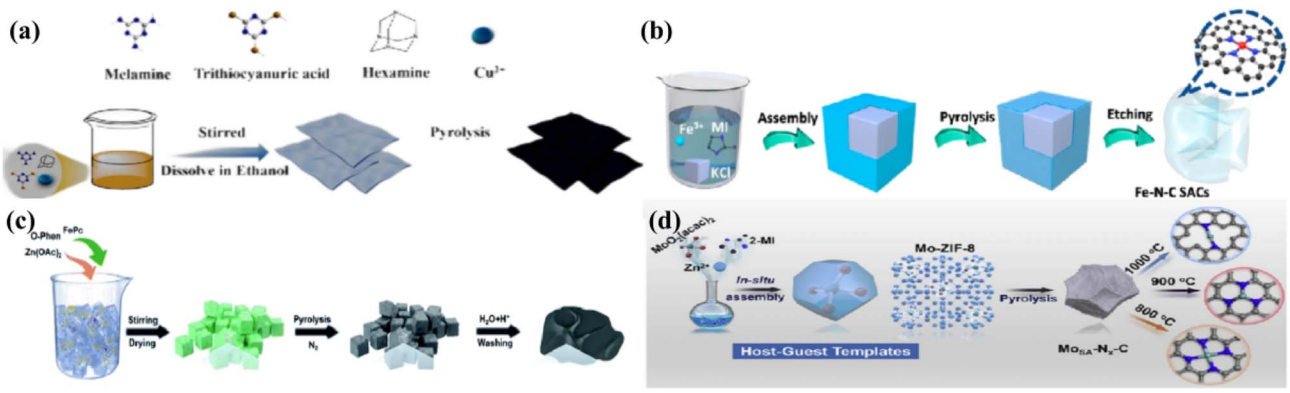

Fig. 4 Synthesis of (a) Cu/CN, (b) Fe–N–C single-atom catalysts (SACs), (c) Fe single-atom nanozymes (Fe-SANs), and (d) Mo single atoms in N-doped carbon (MoSA–N_x–C).

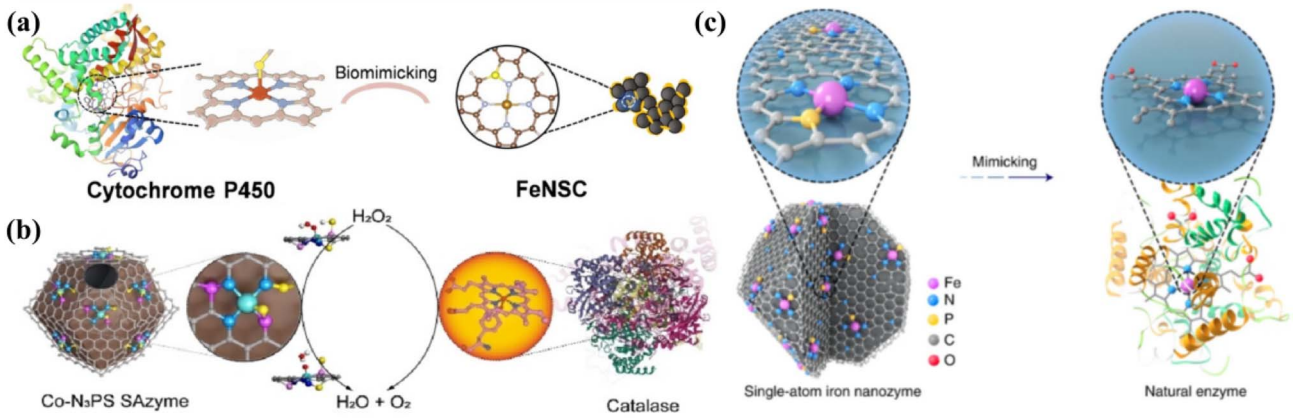

Fig. 5 The bionic design of (a) FeNSC, (b) Fe SAN, and (c) Co-N_3PS.

lower POD-like activity than Fe–N–C. The superior activity of FeN_4 sites originates from their strong H_2O_2 adsorption, lowering the energy barrier for $^{\bullet}OH$ formation.

Biomimetic construction of enzyme-like active sites enhances nanozyme activity and specificity (Fig. 5a–c). Song *et al.*[24] synthesized Cu(II)-modified graphitic carbon nitride (g-C_3N_5–Cu^{2+}), demonstrating a rational design strategy for high-efficiency biomimetic nanozymes. Huang *et al.*[47] prepared cytochrome P450-mimetic FeN_5 SA/CNF (Fig. 5a), exhibiting stronger electron-withdrawing effects than FeN_4 that facilitate O–O bond cleavage and enhance the enzymatic activity. Its catalytic rate constant exceeded commercial Pt/C by 70-fold, conferring antibacterial properties. Remarkably, their encapsulation-pyrolysis strategy extends to Co, Ni, Cu, and Mn atoms, generating thermodynamically stable M-N_5/C structures. Wang *et al.*[48] constructed MoSA–N_x–C (x = 2, 3, 4) (Fig. 4d), demonstrating that atomic configuration tuning *via* coordination number or metal center modification modulates SAzyme activity. Heteroatom substitution (P, S, and Bi) for nitrogen forms Fe/CoN_3P[49,50] (Fig. 5b and c), FeN_3S,[51] FeNBC,[52] and FeN_3Bi[53] compounds. This narrows interatomic distances and enhances substrate interactions. In FeNPC systems, P-doping induces long-range charge transfer that activates metal centers and reduces the energy barrier for ROS formation.[52] Bi-doping creates high-density dual catalytic sites for enhanced activity modulation. In summary, carbon-based nanozymes are classified based on composition and structure, with distinct types offering unique catalytic advantages and broad applicability.

3. Catalytic mechanisms of carbon-based nanozymes

Natural enzyme catalysis, underpinned by transition state theory, involves stabilizing high-energy transition states to reduce activation energy. Analogously, nanozyme catalysis proceeds through three fundamental steps: substrate adsorption, reaction, and product desorption. Based on catalytic function, nanozymes are classified into four types (Fig. 6a): peroxidase (POD), superoxide dismutase (SOD), oxidase (OXD), and catalase (CAT). Carbon-based nanozymes predominantly exhibit POD-like and SOD-like activities. The POD-like mechanism involves hydrogen peroxide (H_2O_2) as an electron acceptor generating hydroxyl radicals ($^{\bullet}OH$). Conversely, some nanozymes function as electron carriers. For SOD-like activity, superoxide anions ($^{\bullet}O_2^-$) coordinate with active sites to form transient complexes that disproportionate to O_2 and H_2O_2 *via* coupled electron/proton transfer.

3.1. Catalytic mechanism of peroxidase (POD)

Peroxidase (POD)-like nanozyme catalysis primarily involves interactions between nanomaterial surface active sites and reactants through three steps: (1) substrate adsorption: active sites (*e.g.*, metal ions and defects) bind to substrates (H_2O_2 and TMB). (2) Electron transfer: mediated by catalytic centers (metal ions/organic cofactors). (3) Product release and cycle regeneration: active sites undergo redox reactions to release products, sustaining catalytic cycles.

Notably, researchers widely recognize hydroxyl radicals ($^{\bullet}OH$) as active intermediates in carbon nanozyme catalytic reactions.[54] However, Yan *et al.*[34] investigated the generation and capture of $^{\bullet}OH$ during the catalytic process of N-CMNs by using electron spin resonance (ESR) spectroscopy and fluorescence spectroscopy, and the results were not consistent with expectations. Therefore, Yan *et al.*[34] speculated that the catalytic mechanism of N-CMNs is similar to that of natural HRP. The high oxidation state intermediate dominates its POD-like catalytic activity, and the catalytic cycle reaction pathway is shown in Fig. 6d. Specifically, steps 1 to 3 represent the adsorption and decomposition processes of H_2O_2, steps 4 to 5 are the transfer processes of proton and electron pairs, and step 6 is the desorption process of H_2O_2. In addition, the catalytic mechanisms of different types of nanozymes are slightly different. The following are some common peroxidase (POD)-like nanozyme materials and their catalytic mechanisms, for instance, carbon quantum dots (CQDs) simulate peroxidase (POD)-like activity through surface functional groups and electron transfer processes.[14] Graphene nanozymes follow a non-free radical mechanism. They adsorb and catalyze the decomposition of

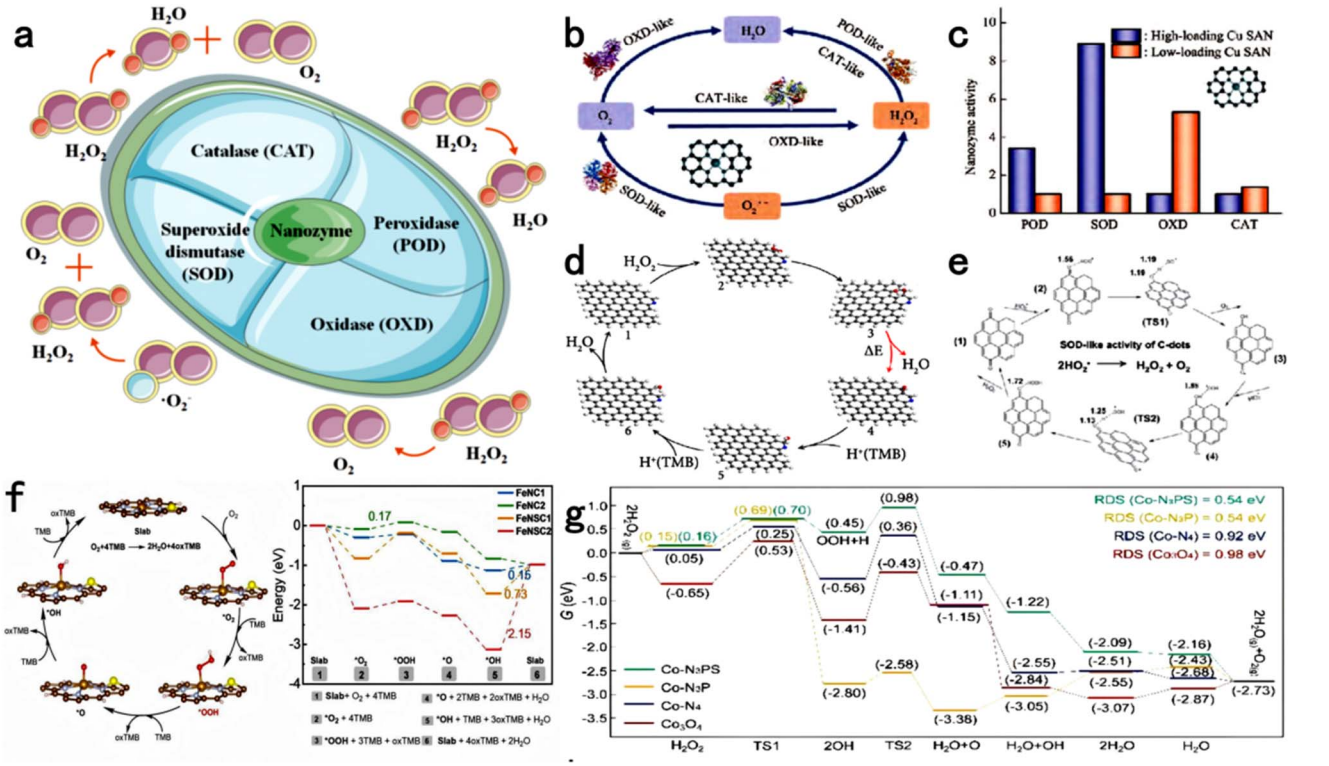

Fig. 6 (a) Schematic of categories of major nanozymes that mediate reactive oxygen species (ROS) homeostasis and oxidative, including CAT-, POD-, OXD- and SOD-mimicking nanozymes. (b) Enzyme type transformation. (c) Nanozyme activity (POD, SOD, OXD, and CAT) of high-loading and low-loading Cu SAN. (d) The process of POD-like catalytic reaction on pyridinic N-doped model graphene. (e) Reaction pathway to achieve the SOD-like catalytic cycle of C-dot nanozymes. (f) Mechanisms and energy profiles for the four-electron oxidation of TMB by O_2 at the FeN_4 site. (g) The free-energy diagrams for catalase-like mechanisms on the four catalyst models of Co-N_3PS, Co-N_3P, CoN_4 and Co_3O_4 under alkaline conditions.

H_2O_2 through surface defect sites and π–π interactions. GO acts as an electron carrier, and when it combines with the amino groups in TMB, it will increase its electron density, which is conducive to electron migration.[24] Metal-supported carbon-based nanozymes, such as Fe–N_x–C, catalyze the decomposition of H_2O_2 to produce hydroxyl radicals (˙OH) through Fenton reactions or Fenton-like reactions[55] and then oxidize reducing substrates such as TMB, ABTS, and OPD.[46,56]

3.2. Catalytic mechanism of superoxide dismutase (SOD)

Natural superoxide dismutase (SOD) catalyzes the disproportionation of superoxide radicals ($^{\cdot}O_2^-$) to O_2 and H_2O_2. Unlike natural SOD, artificial SOD-mimicking nanozymes typically exhibit multimodal antioxidant activities that more efficiently eliminate reactive oxygen species (ROS).[57] Zhang *et al.*[58] demonstrated that Fe–Cu–N_6 single-atom nanozymes significantly surpass natural enzymes in catalytic performance, with exceptional SOD-like selectivity. For C-dot SOD-mimics, Gao *et al.*[59] proposed a catalytic cycle (Fig. 6e) involving seven distinct states of π-conjugated carbonyl groups, including two transition states (TS1/TS2). Hydroxyl-functionalized C-dots exhibit stronger $HO_2^{\cdot}$ radical capture capability due to substantially lower binding energies.

3.3. Catalytic mechanism of oxidase (OXD)

Oxidases (OXD) catalyze hydrogen donor oxidation using O_2 as the electron acceptor, generating H_2O_2 and H_2O in the absence of exogenous H_2O_2.[60] Chen *et al.*[53] verified the role of O_2 in TMB oxidation by purging N_2/O_2 into FeBiNC–TMB systems. Under N_2-saturated conditions, FeBiNC activity increased by 160% (*versus* air) but decreased by 93% under O_2 saturation, confirming the critical role of O_2 in oxidase (OXD)-like catalysis. Xu *et al.*[43] simulated the four-electron reduction mechanism (Fig. 6f). Electron spin resonance revealed ultrahigh O_2 adsorption energy on FeNSC sites, inducing competitive adsorption that facilitates catalytic cycle completion.

3.4. Catalytic mechanism of catalase (CAT)

Catalase decomposes H_2O_2 into H_2O and O_2, protecting cells from ROS-mediated oxidative damage. Thus, catalase (CAT)-like nanozymes alleviate tumor hypoxia as radiosensitizers in cancer therapy.[5] Chen *et al.*[50] proposed a CAT-like mechanism where H_2O_2 adsorption at neutral pH leads to heterolytic cleavage forming ˙OH or homolytic cleavage yielding HOO˙ intermediates (reaction pathway 1: $H_2O_2 \rightarrow {}^{\cdot}OH + OH^-$; pathway 2: $H_2O_2 \rightarrow HOO^{\cdot} + H^+$). These intermediates react with water or O˙ species, ultimately regenerating O_2 and H_2O *via* H abstraction from additional H_2O_2. In addition, catalase (CAT)-like enzymes

exhibit higher activity under neutral or alkaline conditions. By comparing the free energy of the catalase-like catalytic mechanism of four catalyst models, namely Co-N_3PS, Co-N_3P, CoN_4 and Co_3O_4 (Fig. 6g), the results show that the doped S atom has a stronger affinity for the H atom, while the P atom has a stronger affinity for the hydroxyl radical (˙OH). Moreover, the Co–S coordination bond is of great significance to the progress of H_2O_2 dissociation in Co-N_3PS.

3.5. Challenges in the research of catalytic mechanisms

The following are the primary challenges in nanozyme mechanistic studies.

3.5.1. Capturing dynamic evolution of active sites. Heterogeneous atomic arrangements enable the coexistence of active sites (metal coordination centers, edge defects, and oxygen vacancies). During catalysis, these undergo millisecond-to-femtosecond dynamics (coordination shifts, valence changes, and intermediate generation), exceeding the temporal resolution of conventional techniques (TEM, XPS, and EXAFS). For example, tracking Fe^{2+}/Fe^{3+} redox cycling during H_2O_2 decomposition by Fe-carbon nanozymes remains unresolved. Conventional transmission electron microscopy (TEM) struggles to track transient changes in monatomic coordination environments, but recent advances in *in situ* characterization technologies addressed this challenge by quantifying dynamic evolution parameters—including valence states, coordination numbers, and bond lengths. Exemplary breakthroughs include XFEL-XAS with sub-100-fs temporal resolution for capturing ultrafast electronic transitions and environmental TEM (ETEM) enabling real-time observation of single-atom coordination changes at ≈1 nm spatial resolution. Despite such progress, two critical limitations persist: (1) standardization of multimodal technology integration and (2) high-throughput processing of terabyte-scale datasets generated by techniques like XFEL.

3.5.2. Establishing multiscale structure–activity relationships. Disconnects persist between microscale DFT models and macroscale kinetic parameters (*e.g.*, apparent activation energy). Theoretical calculations predict single-site efficiency but neglect aggregation effects and carrier interactions causing activity attenuation. (3) Bridging theoretical and experimental gaps: DFT models adopt idealized systems (pristine surfaces and cluster models), ignoring real-world complexities: surface defects, thermal fluctuations, impurity interference, and solvent effects. A case in point is that while Fe–N_4 sites are predicted as primary active centers in Fe–N–C nanozymes, biological environments induce dynamic reconstruction that alters site reactivity.

4. Fundamental basis for nanozyme catalysis

While diverse nanozymes may exhibit identical catalytic activities, their underlying mechanisms often differ fundamentally. For carbon-based nanozymes, catalytic properties are primarily derived from the following three key attributes: high surface area enabling dense active site exposure, versatile adsorption/loading capacity for catalytic modifiers and superior electron-transfer kinetics that facilitate redox processes.

4.1. Active sites

Carbon-based nanozymes host abundant active sites primarily comprising oxygen-containing functional groups: hydroxyl (–C–OH), carboxyl (–COOH), and carbonyl (–C=O).[59] These surface/defect-bound groups interact with substrates *via* hydrogen bonding or serve as catalytic centers, forming stable active sites. For instance, carbon nanotubes and graphene quantum dots leverage high surface areas for substrate adsorption and catalysis. Gao *et al.*[59] introduced hydroxyl groups (–C–OH), carboxyl groups (HO–C=O), and carbonyl groups (–C=O) on the surface of carbon dots (CDs), endowing them with superoxide dismutase (SOD)-like activity through the synergistic effect of multiple groups. Specifically, the hydroxyl and carboxyl groups combine with the superoxide anion through hydrogen bonds, while the carbonyl group takes electrons from the superoxide anion, thereby generating oxygen and a reduced carbon dot. Subsequently, the reduced carbon dot will then be oxidized by another superoxide anion to produce hydrogen peroxide. The research of Sun *et al.*[61] confirmed that the carboxyl group (HO–C=O) and carbonyl group (–C=O) on the outer surface of GQDs served as the substrate binding site and catalytic active site, respectively, while the hydroxyl group (–C–OH) inhibited its peroxidase (POD)-like activity.

4.2. Electron transfer

Catalytic processes typically involve electron transfer and redox reactions. Consequently, nanozyme activity correlates directly with charge transfer efficiency. Owing to superior conductivity, graphene and carbon nanotubes enable H_2O_2 decomposition by serving as electron carriers, generating ˙OH radicals. For example, graphene oxide (GO) exhibits oxidase-like activity[25] through electron transfer from its valence band to the LUMO (lowest unoccupied molecular orbital) of H_2O_2.

4.3. Synergistic effect

Carbon-based nanozyme activity can be enhanced through heteroatom doping (N, P, and S) or multi-metal loading, which provide additional active sites and improve the catalytic efficiency. For instance, Li *et al.*[44] incorporated sulfur into Fe–N_4–C systems, introducing sulfoxide functional groups (–S=O) onto the carbon plane. This transforms the traditional planar Fe–N_4–C centers into three-dimensional architectures. Studies confirm that these oxidized sulfur groups assist in substrate binding orientation and promote product desorption, yielding specific activity that is 6.8-fold higher than that of Fe–N–C SAzymes.

5. Regulating carbon-based nanozyme performance

Similar to natural enzymes, nanozyme activity depends on the pH and temperature. Nevertheless, their catalytic performance

can be modulated by strategies such as altering their size, morphology, composition, coordination structure, surface modification, interaction with biomolecules, or changing reaction conditions. These performance regulation strategies (size/morphology control, composition tuning, *etc.*) are rigorously implemented by leveraging the fundamental elements—active sites, electron transfer, and synergistic effects—established in Section 4.

5.1. Tailoring the size and morphology

Nanomaterial size and morphology critically influence the catalytic activity. Tuning these parameters optimizes the surface area distribution and active site exposure, thereby enhancing the performance. Typically, smaller nanozymes with higher specific surface areas exhibit greater substrate binding probability and superior catalytic activity. Porous carbon-based nanozymes are commonly synthesized using metal–organic frameworks (MOFs) as sacrificial templates.[62] Controlled carbonization of MOFs enables precise regulation of pore architecture and morphology.

5.2. Engineering the chemical composition

Nanomaterial catalytic activity can be modulated by tailoring the composition and structure. Heteroatom doping (N, P, and S) or phase engineering alters the charge density and induces structural distortion, thereby tuning catalytic performance. Density functional theory (DFT) calculations confirm that defect engineering diversifies nanozyme activities.[63] Introducing P/S heteroatoms to replace coordinating nitrogen forming Fe/CoN_3P[49,50] and FeN_3S[51] enables precise geometric configuration control.

Atomically dispersing active centers maximizes the catalytic efficiency. In carbon-supported single-atom catalysts (SACs), M–N_x–C configurations form stable M–N bonds that mimic natural heme enzymes (*e.g.*, Fe–N_4 of HRP and cytochrome P450). This structural biomimicry achieves near-native enzyme simulation. For instance, inspired by heme cofactors, Li *et al.*[44] incorporated sulfur into Fe–N_4–C, grafting sulfoxide (–S=O) groups onto the carbon plane. This transforms 2D Fe–N_4 sites into 3D architectures, optimizing substrate interaction geometries.

5.3. Implementing surface modifications

Catalytic reactions occur primarily on nanozyme surfaces. Modifying surfaces with coordinating components, functional groups, or polymers enhances substrate binding, significantly altering the activity and selectivity. For example, Chen *et al.*[64] immobilized Pt clusters on layered Fe–N–C carriers, synthesizing FeSA–PtC conjugates with 4.5-fold higher peroxidase-like activity than Fe–N–C and 7-fold higher than Pt clusters. DFT calculations attributed this to electron transfer from Pt clusters to Fe single-atom sites (not *vice versa*), enhancing O–O bond cleavage. Liu *et al.*[65] confirmed that carboxyl, hydroxyl, and amino groups on carbon dots govern SOD-like activity through radical quenching experiments. Huo *et al.*[66] synthesized PSAF NCs *via* ZIF-8 pyrolysis and PEG modification. These selectively trigger Fenton reactions in acidic tumor microenvironments (TME), generating cytotoxic $^{\bullet}OH$ for tumor therapy.

5.4. Tuning interactions with biomolecules

Biomolecular interactions modulate nanozyme catalytic activity. Specifically, conjugating proteins or DNA regulates nanozyme activity and stability. Li *et al.*[67] demonstrated this by anchoring ferroheme (hemin) onto Zn–N–C single-atom nanozymes to construct Zn–N–C@heme SAzymes, which detect propyl gallate (PG) and formaldehyde (HCHO) *via* peroxidase (POD)-like activity. Mechanistically, in the presence of H_2O_2, the SAzyme catalyzes the oxidation of colorless PG to a yellow quinone product and HCHO competitively inhibits this reaction by binding to the active site. This principle establishes a dual-analyte detection platform for PG and HCHO.

5.5. Optimizing reaction conditions

Nanozyme catalytic activity is modulated by external environmental factors, including the pH, temperature, and ionic strength. Optimizing these parameters enhances the catalytic efficiency. Among these, pH exerts the most significant influence, thus shifting pH values fundamentally alters activity profiles and enzyme-mimicking types. Experimental evidence confirms acidic conditions favor peroxidase (POD)-like activity, while neutral/alkaline conditions enhance superoxide dismutase (SOD)-like and catalase (CAT)-like activities.[68]

5.6. Current challenges in regulating nanozyme performance

However, these regulatory strategies face the following key challenges: (1) size-dependent activity enhancement involves inherent trade-offs, with nanoscale dimensions boosting the activity *via* the increased surface area but reducing structural stability. (2) Electron transfer mechanisms, governed by composition/surface modifications, remain elusive due to hybrid system complexity. Precisely tracking electron paths and quantifying synergy are challenging. (3) Biomolecular/environmental regulation exhibits strong pH/temperature dependence. Consequently, most nanozymes function optimally only under specific conditions, which constrains their physiological adaptability and application scope.

6. Applications of carbon-based nanozymes

Carbon-based nanozymes exhibit broad applications across environmental engineering, biosensing, and biomedicine. Specifically, carbon-based nanozymes excel at biosensing and are capable of detecting small molecules, proteins, viruses, and cells. In the environmental field, carbon-based nanozymes are mainly used for the detection and degradation of various pollutants, such as organic dyes, heavy metal ions, antibiotics, *etc.* In the field of biomedicine, carbon-based nanozymes can catalyze reactions to produce reactive oxygen species (ROS), thereby achieving the purpose of antibacterial and killing tumor

cells. Thus, they hold significant potential for integrated sensing, diagnostics, and therapeutics.

6.1. Field of environmental engineering

Carbon-based nanozymes enable sensitive detection and efficient degradation of environmental pollutants,[2,7] including heavy metal ions, like Pb(II), Hg(II), and Cr(VI), and organic pollutants, such as phenolic compounds, antibiotics (*e.g.*, tetracycline), and pesticides (*e.g.*, glyphosate). These compounds constitute major sources of soil and water contamination. Conventional remediation technologies (physical adsorption, chemical oxidation, and bioremediation) face persistent limitations: oxide byproduct generation, high operational costs, poor reaction selectivity and limited recyclability. Nanozymes overcome these constraints owing to their exceptional physicochemical properties—including high specific surface area, enhanced adsorption capacity, abundant catalytic active sites, robust stability, and strong toxicant resistance—enabling efficient ROS-mediated degradation of textile dyes, antibiotics, and pesticide residues.

6.1.1. Detection of heavy metals. Nanozyme-based sensors rely on surface-mediated interactions with specific metal ions to regulate catalytic activity, enabling heavy metal detection. Qi *et al.*[69] leveraged Cr(VI)-8-hydroxyquinoline (8-HQ) complexation to restore TMB oxidation activity (Fig. 7a), achieving Cr(VI) detection *via* chromogenic signal recovery. Wang *et al.*[70] synthesized graphitic carbon nitride–gold nanocomposites (g-C_3N_4–Au) with peroxidase (POD)-like activity. These enabled Hg(II) detection at physiological pH with 0.9 nM sensitivity using colorimetry (Fig. 7b). Such nanosensors offer portable, simple, and ultrasensitive on-site screening using UV-vis spectrophotometers.

6.1.2. Detection of organic pollutants. Nanozyme sensors enable sensitive and selective detection of trace organic pollutants. For example, Boruah *et al.*[71] synthesized dual photo-/magneto-responsive Fe_3O_4–TiO_2/graphene nanocomposites exhibiting synergistic peroxidase (POD)-like and photocatalytic activities. It not only demonstrates highly sensitive colorimetric detection ability for pesticides in water medium but also degrades pesticides in environmental water bodies under light conditions due to its excellent photocatalytic performance.

6.1.3. Degradation of organic dyes. Carbon-based nanozymes degrade dye chromophores primarily through surface-enriched reactive oxygen species (ROS). Unlike conventional photocatalysis requiring pre-activation steps, these ROS exhibit broad-spectrum degradation capabilities toward complex-structured organic dyes due to their inherent oxidative reactivity. This mechanism drives efficient Fenton-like reactions under ambient conditions. Although traditional Fenton catalysts rely on transition metal centers (*e.g.*, Fe, Cu, and Mn), transition metal-doped carbon single-atom nanozymes (SAzymes) significantly enhance reaction kinetics. Table 1 summarizes key kinetic parameters of such SAzymes in pollutant degradation.

Carbon-based nanozymes mimic peroxidase activity by catalyzing H_2O_2 decomposition to generate hydroxyl radicals ($^{\bullet}OH$), oxidizing organic dyes.[78,79] Chen *et al.*[80] synthesized Fe/Cu–N–C single-atom nanozymes *via* folic acid-templated pyrolysis. This layered material degrades Rhodamine B (RhB) in environmental matrices (Fig. 7c), demonstrating wastewater treatment potential. Chen *et al.*[53] doped Fe into Bi-MOF and then carried out high-temperature pyrolysis to form the FeBi-NC

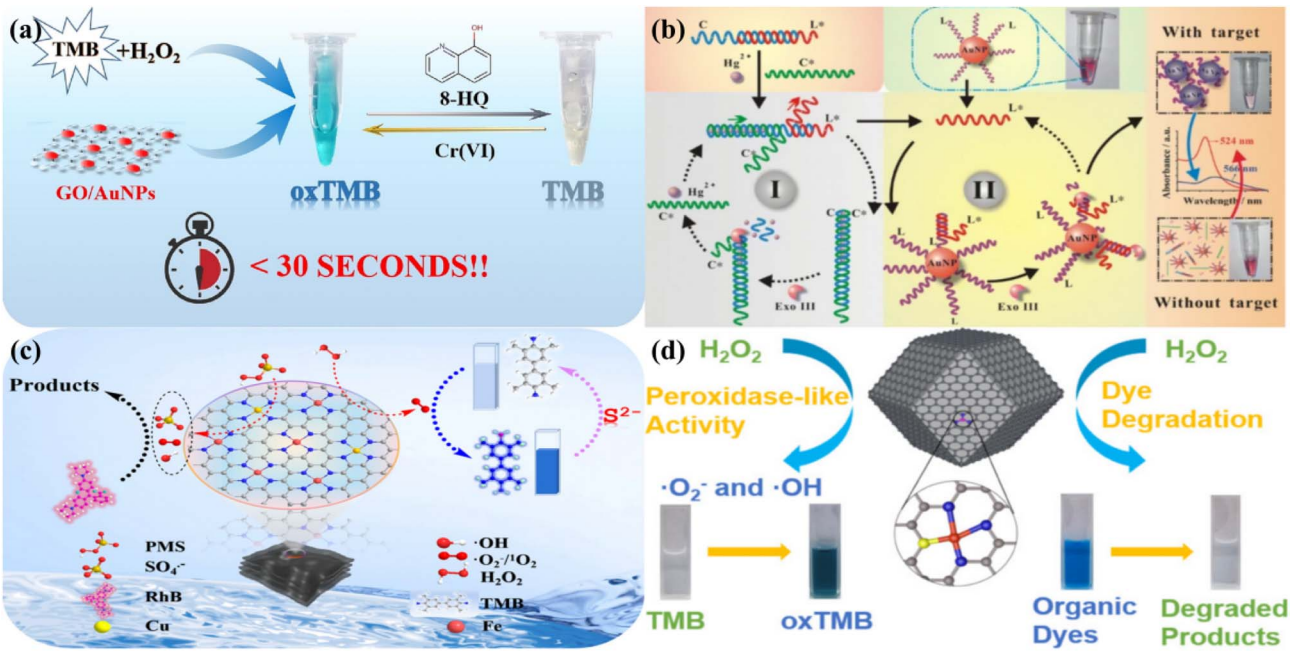

Fig. 7 Schematic diagram of (a) ultrafast colorimetric detection of Cr(VI) based on GO/AuNPs. (b) Colorimetric detection of Hg(II) based on g-C_3N_4–Au. (c) Detection of S^{2-} and degradation of RhB based on Fe/Cu-NC. (d) Degradation of MB based on a Mn-SAzyme.

Table 1 Kinetic comparison of catalysts for organic pollutant degradation activated by PMS/H_2O_2

Nanozyme (g L^{-1})	Pollutant (mg L^{-1})	Activation (g L^{-1} M^{-1})	k (min^{-1})	k_{nor} (min^{-1} g^{-1} L)	Ref.
FeCo-NC-1,0.1	BPA,20	PMS,0.2	1.179	11.79	72
FeCo-NC-2,0.1	BPA,20	PMS,0.2	1.252	12.52	
FeCo-NC-3,0.1	BPA,20	PMS,0.2	0.465	4.65	
Bi-NC,0.03	RhB,10	PMS,15	0.467	15.57	73
Fe-NC,0.03	RhB,10	PMS,15	0.505	16.83	
FeBi-NC,0.03	RhB,10	PMS,15	0.733	24.43	
Fe/Cu-NC,2	MG,10	PMS,30	0.8218	0.411	74
Fe/Cu-NC,2	MB,10	PMS,30	0.5702	0.285	
Fe/Cu-NC,2	RhB,10	PMS,30	0.5943	0.297	
γ-Fe_2O_3/Mn_3O_4,0.05	RhB	PMS,50	—	—	75
Mn-SAzyme,0.025	MB,10	H_2O_2,0.1	~0.0096	~0.384	76
Mn-SAzyme,0.025	RhB,10	H_2O_2,0.1	<0.0096	<0.384	
MOF-545(Fe),10	MO,10	H_2O_2,0.1	—	—	77
MOF-545(Fe),10	MB,10	H_2O_2,0.1	—	—	

SAzyme. The dual-site single-atom nanozyme, featuring Fe–N_4 and Bi–N_4, is loaded on a carbon matrix. This nanozyme can be used in multi-step catalytic reactions. In other words, redox reactions and activation of persulfate to efficiently degrade the organic dye Rhodamine B. This cascaded catalytic characteristic enables it to play an important role in environmental remediation and wastewater treatment. Feng *et al.*[81] synthesized a Mn-SAzyme with metallic manganese as the active center. In this study, based on the Fenton-like reaction, methylene blue (MB) was used as the organic dye model (Fig. 7d), and the Mn-SAzyme was used as the catalyst. The degradation rate of methylene blue could reach 90.1% within 300 minutes under the given reaction conditions. Nanozymes exhibit higher catalytic activity and stability than natural enzymes in the degradation process of organic dyes while maintaining efficient catalytic performance under complex environmental conditions. In addition, nanozymes can exert excellent catalytic activity under mild conditions, including normal temperature, pressure and near-neutral pH conditions, thereby reducing the negative impact on the environment. Furthermore, nanozymes usually have good recyclability and reusability, reducing degradation costs and enhancing feasibility in practical applications. In conclusion, nanozymes have demonstrated high efficiency, stability, and environmental friendliness in the degradation of organic dye, providing a promising strategy for solving the problem of organic dye pollution.

6.1.4. Degradation of antibiotics. Nanozymes enable efficient antibiotic degradation by leveraging unique nanomaterial properties and catalytic activities. Carbon-based nanozymes drive preferential degradation of labile bonds in antibiotic pharmacophores (*e.g.*, β-lactam rings in penicillins and quinolone cores in fluoroquinolones) through localized ROS generation. This site-specific oxidative cleavage initiates deep mineralization pathways, critically suppressing resistance gene dissemination by eliminating antibiotic selection pressure. Xie *et al.*[82] synthesized 3D hollow porous FeCu–N–C with dual Fe–N_x/Cu–N_x sites *via* salt-templating/freeze-drying. This activates persulfate (PS) to degrade levofloxacin (LEV) with 90.4% efficiency within 30 min. Wang *et al.*[83] integrated single-atom nanozymes into ceramic membranes and successfully prepared Fe–SA–N_3/CM with high hydrophilicity. Employing this material as a catalyst, they achieved the selective, continuous and stable degradation of cephalosporins. In conclusion, nanozymes have demonstrated high efficiency, broad-spectrum performance, and low drug resistance in antibiotic degradation, offering novel strategies for addressing the issues of antibiotic contamination and drug resistance.

6.2. Field of biosensing

Biosensors based on carbon-based enzyme-like materials have been successfully applied to detect H_2O_2 and small biomolecules that can release H_2O_2, such as glucose[24] and choline.[52] They have also been used to detect other reducing small biomolecules like ascorbic acid, cysteine, biothiols, and tumor markers.

6.2.1. Detection of H_2O_2 and H_2O_2-generating biomolecules. Leveraging the peroxidase (POD)-like activity of nanozymes, H_2O_2 is catalytically converted to hydroxyl radicals (˙OH) that oxidize chromogenic substrates (TMB, ABTS, OPD, and AR), enabling colorimetric detection of free H_2O_2 and biomolecules generating H_2O_2 (*e.g.*, glucose, xanthine, and choline *via* oxidase enzymes). Jiao *et al.*[84] used Fe–N–C nanozymes to detect intracellular H_2O_2 in HeLa cells by oxidizing TMB to blue oxTMB (Fig. 8a). Song *et al.*[24] developed GO–COOH–based glucose sensors with an LOD of 0.5 μM in blood/juice samples. Jiao *et al.*[52] achieved organophosphate pesticide detection *via* acetylcholinesterase inhibition assays using FeBNC (Fig. 8b). Based on this principle, Cheng *et al.*,[55] Wang *et al.*,[48] and Wu *et al.*[85] prepared CNT/FeNC, MoSA–N_3–C, and Cu–N–C, respectively, with excellent peroxidase (POD)-like activity and successfully achieved rapid colorimetric detection of glucose, xanthine, choline, and organophosphorus pesticides.

6.2.2. Detection of antioxidants. Carbon-based nanozymes harness peroxidase (POD)-like activity to catalyze H_2O_2 into hydroxyl radicals (˙OH), oxidizing chromogenic substrates like TMB for colorimetric sensing. In such systems, antioxidants inhibit signal generation either by competing for nanozyme

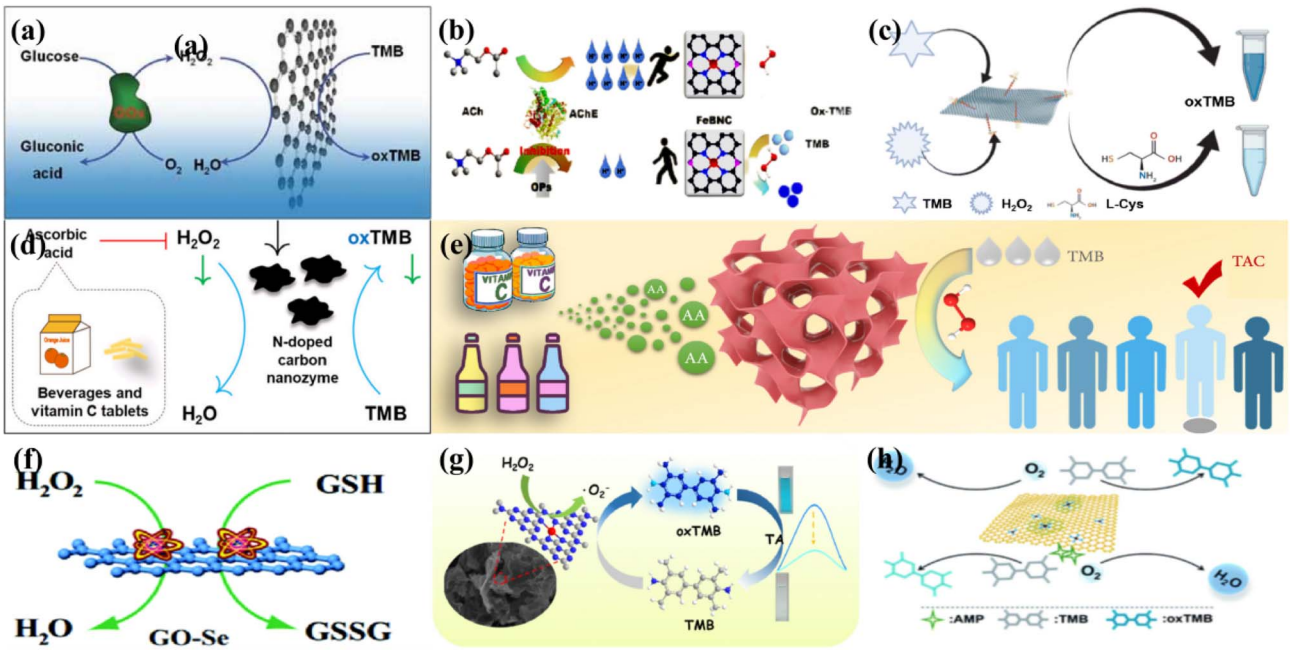

Fig. 8 Schematic illustrations of (a) glucose detection *via* the GO-COOH catalytic reaction; (b) AChE activity and OP (organophosphorus pesticide) sensing; (c) L-cysteine colorimetric detection using rGO-GP; (d) ascorbic acid detection with N-doped carbon nanozymes; (e) total antioxidant capacity (TAC) assay using NP-CMNs; (f) H_2O_2 removal mechanism by GPX-like GO–Se; (g) colorimetric TA (tannic acid) detection principle; (h) AMP (4-acetaminophen) detection principle.

active sites or scavenging ˙OH/peroxides, thereby attenuating substrate oxidation and enabling spectrophotometric quantification. Key advances include the following: Dugan *et al.*[22] synthesized polysaccharide-modified rGO-GP *via* hydrothermal reduction, developing a serum L-cysteine sensor (Fig. 8c) with diagnostic potential. Lou *et al.*[33] achieved multi-analyte detection (H_2O_2, glucose, and ascorbic acid) using high-N-doped carbon nanozymes (Fig. 8d). Yan *et al.*[34] engineered pyridinic-N-tuned porous nanozymes for total antioxidant capacity (TAC) assays in food/healthcare (Fig. 8e). Chen *et al.*[37] demonstrated N,S-co-doped porous carbon, exhibiting 3.9-fold enhanced activity and 11.8-fold higher H_2O_2 affinity *versus* N-doped controls, enabling beverage TAC detection, and Xie *et al.*[42] utilized Cu/CN single-atom nanosheets for ultrasensitive tea antioxidant analysis (LOD = 30 nM, Fig. 8g), guiding high-density active site design. Similarly, Wu *et al.*[45] leveraged paracetamol's inhibition of Fe-SAN oxidase to develop nanozyme-inhibition-based drug detection (Fig. 8h), revealing inhibitor–nanozyme interaction mechanisms. These systems enable detection of diverse reductants, including ascorbic acid, glutathione,[36] cysteine, and dopamine through signal modulation principles. In addition, the inhibition mechanism of certain enzymes assessed *via* carbon nano-enzyme colorimetry resembles that described for antioxidant detection. For example, acetylcholinesterase (AChE)—a key enzyme linked to neurological disorders like Alzheimer's's disease—is quantitatively detected by leveraging the inhibitory effect of nanozymes on chromogenic reactions. This inhibition alters the catalytic oxidation of hydrolysis products derived from AChE activity, generating measurable signals.[86,87]

6.2.3. Detection of tumor markers. Nanozymes detect tumor markers by mimicking natural enzyme catalysis, offering superior stability in complex biological environments and facilitating surface modification. For example, Xu *et al.*[88] developed a nanozyme-based ELISA using Fe–N_4Cl/CNCl for colorimetric carcinoembryonic antigen detection, achieving 7-fold lower detection limits than conventional horseradish peroxidase (HRP)-ELISA while simultaneously inhibiting tumor growth *in vitro* and *in vivo*; Song *et al.*[89] synthesized folate-conjugated graphene–heme complexes (GFH) that quantitatively detect cancer cells *via* a linear correlation between the cell count and GFH-bound absorbance (R^2 = 0.99). These systems demonstrate two key advantages: (1) high sensitivity/specificity for early cancer screening (AUC > 0.95 in clinical validation); (2) integrability with nanotechnology platforms (*e.g.*, electrochemical biosensors and microfluidics), enabling scalable clinical diagnostic applications.

6.3. Field of biomedicine

Carbon-based nanozymes exhibit promising biomedical applications, including cancer therapy, anti-inflammatory/antibacterial treatment, wound disinfection, cellular protection, and bioimaging.

6.3.1. Antioxidant and anti-inflammatory treatments. Nanozymes address the instability of endogenous antioxidant enzymes (*e.g.*, catalase and SOD) in pathological conditions by mimicking catalytic ROS regulation. Ma *et al.*[90] constructed Fe–N_4-centered Fe–SAs/NC *via* FePc@ZIF-8 pyrolysis, exhibiting dual CAT/SOD-like activities that eliminate intracellular ROS to protect cells from oxidative stress. Cao *et al.*[91] engineered tri-

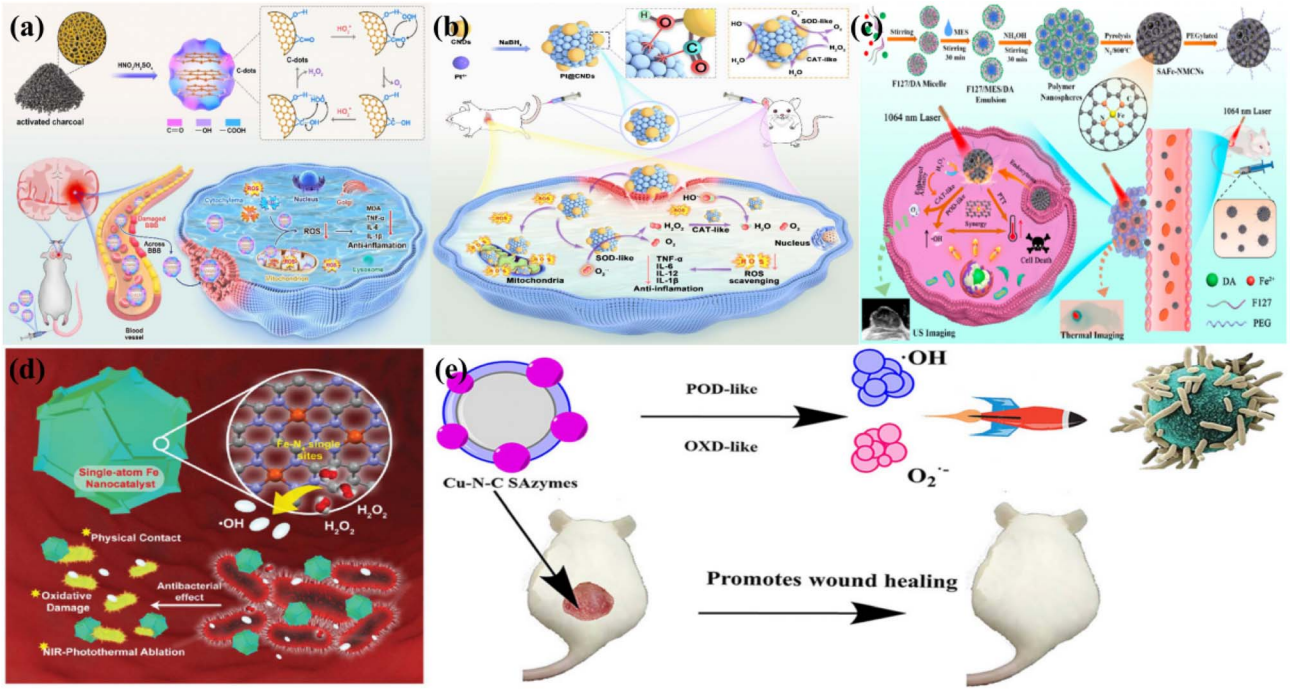

Fig. 9 Schematic illustrations of (a) C-dot SOD-mimetic nanozyme synthesis and ischemic stroke therapy, (b) Pt@CNDs cascaded nanozyme synthesis and intracellular ROS elimination, (c) synergistic tumor therapy mechanism of dual enzyme-mimic SAFe-NMCNs, (d) antibacterial mechanism of SAFe NCs, and (e) antibacterial and wound healing actions of the Cu–N–C nanozyme.

enzyme mimetic (SOD/CAT/GP$_x$) Co single-atom catalysts that scavenge ROS/RNS, alleviating sepsis *via* $^{\bullet}O_2^-$ and H_2O_2 decomposition. Gao *et al.*[59] designed multi-group-functionalized carbon dots (CDs, Fig. 9a) with ultrahigh SOD-like activity, enabling mitochondrial-targeted ROS identification and demonstrating therapeutic potential for ischemic stroke; Zhang *et al.*[92] synthesized Pt@CNDs (Fig. 9b) by integrating SOD-mimetic carbon nanodots (CNDs) with Pt nanoparticles, which catalytically convert toxic H_2O_2 to H_2O/O_2 while exhibiting cascade-amplified anti-inflammatory effects *in vivo*.

6.3.2. Tumor and cancer treatment. Catalytic tumor therapy utilizing enzyme-mimicking nanozymes is an emerging strategy with cost efficiency and stability advantages.[93] The biocompatible carbon matrix enhances biological safety, expanding biomedical applications. Current nanozyme-based therapeutic modalities include chemodynamic therapy (CDT),[66] photothermal therapy (PTT),[94,95] and photodynamic therapy (PDT).[96] Among the above-mentioned treatment strategies, the principle is that nanozymes generate highly toxic reactive oxygen species (ROS), mainly $^{\bullet}O_2^-$ and $^{\bullet}OH$, by catalyzing oxidants such as O_2 or H_2O_2, or by irradiating photosensitizers with light to produce ROS, thereby triggering apoptosis or necrosis of tumor cells. Among them, chemodynamic therapy (CDT) is based on a Fenton-like reaction to catalyze the generation of hydroxyl radicals ($^{\bullet}OH$) from hydrogen peroxide in a weakly acidic tumor microenvironment with excessive hydrogen peroxide thereby causing apoptosis of tumor cells. Based on the high permeability and retention effect (EPR) of tumors, Huo *et al.*[66] utilized PSAF NCs to accumulate them in tumor lesions. Under the conditions of excessive weak acid and hydrogen peroxide, they catalyzed the generation of hydroxyl radicals ($^{\bullet}OH$) to induce the accumulation of lipid peroxides and inhibit tumor growth and ferroptosis. Cai *et al.*[97] synthesized Co–SAs@NC, which can initiate a cascade of enzymatic reactions for tumor catalytic therapy. This nanozyme first exerts its catalase-like activity to decompose endogenous hydrogen peroxide in tumor cells into oxygen and then utilizes its catalase-like activity to reduce oxygen to superoxide anion radicals ($^{\bullet}O_2^-$), thereby triggering apoptosis of tumor cells. If further combined with chemotherapeutic drugs, such as doxorubicin, its anti-tumor effect can be significantly enhanced. Photothermal therapy (PTT) refers to a treatment method in which, under laser irradiation, photothermal conversion materials use the heat generated by photothermal conversion to kill cancer cells. Compared with traditional treatment methods such as chemotherapy and radiotherapy, photothermal therapy (PTT) is more efficient, precise and controllable. Furthermore, integrating photothermal therapy (PTT) with targeted drug delivery using photothermal-responsive nanocarriers blocks oncogenic signaling pathways while thermally ablating tumors, synergistically enhancing treatment efficacy.[98,99] Su *et al.*[94] synthesized SAFe-NMCNs by loading iron single atoms on nitrogen-doped mesoporous carbon nanospheres. This nanozyme can have the activities of dual enzymes, including catalase (CAT) and peroxidase (POD). Therefore, based on SAFe-NMCNs, not only can ultrasound imaging of the tumor site be achieved, but also hydrogen peroxide can be catalyzed to generate hydroxyl radicals ($^{\bullet}OH$) for tumor cell apoptosis (Fig. 9c). Importantly, this material has excellent photothermal properties and can achieve photothermal enhancement of tumor therapeutic effects.

Photodynamic therapy (PDT) involves irradiating photosensitizers in tumor tissues with light of specific wavelengths, thereby generating reactive oxygen species to kill tumor cells.

6.3.3. Antibacterial and antiviral treatment. Nanozymes provide potent alternatives to traditional antibiotics by circumventing drug resistance *via* ROS-mediated mechanisms. Leveraging their oxidase/peroxidase (POD)-like activities, they catalyze H_2O_2 or activate O_2 to generate reactive oxygen species (ROS), achieving broad-spectrum efficacy against bacteria (*e.g.*, *Staphylococcus aureus*), fungi, and viruses. Key demonstrations include: Wang *et al.*[25] engineered peroxidase-mimetic oxidized carbon nanotubes (o-CNTs) that eliminate wound infections under physiological conditions by catalyzing trace $H_2O_2 \rightarrow {}^{\bullet}OH$, avoiding high-concentration H_2O_2 side effects. Huo *et al.*[100] utilized Fe single-atom nanozymes (SAFe NCs) with dual peroxidase-like/photothermal properties (Fig. 9d) to eradicate Gram positive (*S. aureus*) and Gram negative (*E. coli*) bacteria *via* ROS generation combined with 808 nm NIR irradiation (>99.9% disinfection rate); Zhu *et al.*[101] synthesized Cu–N–C single-atom nanozymes exhibiting enhanced antibacterial activity under light activation (Fig. 9e) and validated by biocompatibility assays (MTT, hemolysis, and blood analysis); and Tripathi *et al.*[39] developed N,P,S-co-doped carbon quantum dots (NSP-CQDs) with multifunctional antibacterial activity against pathogenic strains.

6.3.4. Intervention in neurological disorders. Carbon-based nanozymes, as emerging nanotherapeutic agents, demonstrate unique advantages for neurological disorder intervention, particularly in regulating histone deacetylase (HDAC).[102] Conditions like Alzheimer's disease, Parkinson's disease, and stroke often involve abnormal HDAC expression/activity, leading to gene dysregulation and neuronal dysfunction.

Leveraging their tunable enzyme-like activity, high stability, and multifunctional synergy, carbon-based nanozymes implement HDAC modulation through direct inhibition mechanisms. Studies confirm that nitrogen-containing functional groups (*e.g.*, pyridinic-N and graphitic-N) on N-doped nanozymes bind Zn(II) in HDAC catalytic centers, blocking enzymatic function.[103,104] This inhibition exhibits subtype selectivity; for instance, S-doped nanozymes show enhanced HDAC6 affinity,[105] attributed to specific interactions between sulfur atoms and HDAC6's zinc-finger ubiquitin-binding domain (ZnF-UBP) within its dual-catalytic domains (CD1/CD2).

6.3.5. Biological imaging. Nanozymes function as multifunctional therapeutic agents enabling tumor tracking, microenvironment modulation, and integrated cancer diagnosis/therapy.[12] By synergizing inherent optical/thermal/electrical properties with imaging modalities, fluorescence,[65,106] MRI,[107] photothermal,[12,94,107] ultrasound,[108] and computed tomography (CT),[11,108] they facilitate novel sensing platforms. Currently, the application research of the integration of nanozymes and fluorescence imaging technology is relatively extensive, while the development of other integrated technologies is relatively slow. Specifically, in fluorescence imaging, nanozymes generate fluorescence signals by catalyzing fluorescent substances to achieve the detection and imaging of specific biomarkers. For instance, Liu *et al.*[65] developed a novel type of superoxide dismutase (SOD) nanoenzyme fluorescent carbon dot (C-dot), with a fluorescence emission wavelength of 683 nm, an absolute quantum yield as high as 14%, and showed SOD enzyme activity exceeding 4000 U mg^{-1}. This offers great potential for imaging the biological distribution of nanozymes themselves *in vivo* and for treating inflammatory diseases. Ma *et al.*[106] synthesized a multifunctional carbon dot nanomaterial using glutathione and biotin. This carbon dot not only exhibited excellent superoxide dismutase (SOD)-like activity, that is, hydroxyl radical scavenging ability, but also possessed fluorescence properties. Therefore, in the IBD model, this nanozyme can not only improve intestinal inflammation but also be used for *in vivo* fluorescence imaging of the intestine. In nuclear magnetic resonance technology, nanozymes are used as contrast agents to achieve the purpose of real-time imaging. In photothermal imaging, nanozymes combine photothermal technology to achieve imaging of tumor and other lesion tissues and evaluation of therapeutic effects through the heat generated by catalytic reactions. For instance, Lu *et al.*[107] successfully constructed the bionic enzyme MC–Mn that can guide dual-mode imaging. This enzyme has a high photothermal conversion efficiency and drug loading performance. On the one hand, MC–Mn can be used as a photothermal carrier to load photosensitizing agents. On the other hand, this enzyme can also be used as a contrast agent in magnetic resonance imaging (MRI) to achieve real-time imaging of tumors. In ultrasound imaging,[108] nanozymes are combined with ultrasound technology to achieve the imaging of deep tissues through the bubbles or acoustic wave signals generated by catalytic reactions. In photothermal imaging,[12,94] nanozymes combine photothermal technology to achieve imaging of tumors and other lesion tissues and evaluation of therapeutic effects through the heat generated by catalytic reactions. In CT imaging,[11,108] the contrast of CT images is enhanced through catalysis, thereby improving the resolution of the imaging. Multimodal integration remains promising for expanding clinical diagnostics.

6.4. Adaptation challenges in practical Applications

Nanozymes face three key implementation barriers:

- Complex matrix interference: in biosensing applications (*e.g.*, blood analysis), endogenous components like proteins and ions inhibit nanozyme catalytic activity, compromising detection accuracy. Similarly, complex environmental matrices impair pollutant degradation efficiency in aqueous remediation systems. Critically, comprehensive datasets on nanozyme environmental persistence and ecotoxicological risks remain scarce.
- Biocompatibility–activity trade-off: the optimal equilibrium between biocompatibility and catalytic efficacy remains elusive. Key unresolved challenges include: undefined *in vivo* metabolic pathways, precious metal-induced cytotoxicity (*e.g.*, mitochondrial apoptosis), and scarce long-term biosafety data (>6 months exposure models). This fundamental conflict severely restrains clinical translation.
- Lack of standardization: a unified evaluation framework is absent, leading to inconsistent testing protocols across studies.

Critical metrics—including Michaelis constants (K_m) and turnover frequencies (k_{cat})—lack standardized assay methodologies, severely compromising cross-study comparability.

7. Conclusion

While carbon-based nanozymes demonstrate marked advantages over natural enzymes in terms of cost efficiency[109] (>100-fold reduction), scalable production,[110] extended storage stability[109] (≥5 months[110,111]), and robustness under harsh conditions,[112] three fundamental limitations persist: inferior activity and specificity compared to natural enzymes (k_{cat}/K_m values <15–20%[113] of native analogs), limited enzyme-mimic diversity (with >90% studies focused on oxidoreductases *versus* <5% on transferases, lyases, ligases, and isomerases[114]), and unresolved recyclability[115] (showing >90% activity loss after 5 reuse cycles[111,116]).

The heterogeneity of material structures leads to divergent catalytic mechanisms, while atomic-scale reaction pathways with definitive structure–activity relationships require further elucidation (see Section 3). Although Section 5 outlines performance modulation strategies, current synthesis methods fail to precisely control active-site density (<±10% variance) and coordination environments (*e.g.*, M–N_4 *versus* M–N_2O_2 configurations), necessitating universal synthetic protocols, and sensing applications dominate research (>70% of publications[117]), yet large-scale *in vivo* behavior studies remain scarce (<5% of studies report pharmacokinetics[118,119]). Critically, the mismatch between optimized catalytic conditions (*e.g.*, pH 4.5) and physiological environments (pH 7.4) exacerbates unresolved biocompatibility challenges (Section 6), demanding interdisciplinary convergence across computational modeling, surface science, and nanotoxicology.

Nanozyme research and application require establishing standards such as ISO-compliant testing protocols with defined reaction conditions and substrate ranges. Concurrently, advanced fundamental research infrastructure (*e.g.*, *in situ* characterization platforms) and scaling instrumentation are paramount to build a vertically integrated nanozyme value chain spanning innovation discovery, industrial production, and clinical translation.

In summary, this work highlights carbon-based nanozymes as transformative catalytic platforms, demonstrating quantifiable advancements in sustainability (reducing enzyme production costs by >90%[34]) and multimodal therapeutic efficacy (*e.g.*, ROS generation rates >50 μM min^{-1}). These innovations establish foundational frameworks for next-generation nanobiocatalysts, with proven versatility in environmental remediation, precision diagnostics, and targeted therapeutics. Their continued evolution will catalyze cross-disciplinary convergence across materials science, synthetic biology, and nanomedicine, positioning this field in the vanguard of sustainable nanotechnology innovation.

Data availability

All relevant data are within the manuscript and its additional files.

Conflicts of interest

The authors declare that they have no known competing financial interests or personal relationships that could have appeared to influence the study reported in this document.

Acknowledgements

We are thankful for financial support from Guangxi Key Laboratory of Electrochemical and Magnetochemical Functional Materials, National Natural Science Foundation of China (No. 21565011), the Guangxi Key Laboratory of Environmental Pollution Control Theory and Technology, and Guangxi Colleges and Universities Key Laboratory of Food Safety and Detection.

References

1 W. L. Li and T. Head-Gordon, *ACS Cent. Sci.*, 2021, **7**, 72–80.
2 R. Singh, A. Umapathi, G. Patel, C. Patra, U. Malik, S. K. Bhargava and H. K. Daima, *Sci. Total Environ.*, 2023, **854**, 158771.
3 L. H. Shen, D. X. Ye, H. B. Zhao and J. J. Zhang, *Anal. Chem.*, 2021, **93**, 1221–1231.
4 J. Shen, J. Chen, Y. P. Qian, X. Q. Wang, D. S. Wang, H. G. Pan and Y. G. Wang, *Adv. Mater.*, 2024, **36**, 2313406.
5 G. J. Hou, Y. K. Xu, C. H. Wang, C. Lu, A. Thakur, K. Zhang, W. Li and Z. J. Xu, *Aging Dis.*, 2025, DOI: **10.14336/AD.2025.0011**.
6 X. Ma, G. Sun, A. Leng, X. Wei, J. Xu, W. Ding, H. Liu and H. Fang, *Talanta*, 2025, **296**, 128398.
7 A. Das, R. V. S. Uppaluri and S. Mitra, *Chem. Eng. J.*, 2025, **507**, 160762.
8 E. Z. Gomaa, *J. Cluster Sci.*, 2022, **33**, 1275–1297.
9 A. M. Ashrafi, Z. Bytesnikova, J. Barek, L. Richtera and V. Adam, *Biosens. Bioelectron.*, 2021, **192**, 113494.
10 L. Feng, M. C. Zhang and Z. Y. Fan, *Anal. Methods*, 2024, **16**, 6771–6792.
11 X. D. Zhang, X. K. Chen and Y. L. Zhao, *Nano-Micro Lett.*, 2022, **14**, 165–191.
12 M. Cordani, J. Fernández-Lucas, A. Khosravi, E. N. Zare, P. Makvandi, A. Zarrabi and S. Iravani, *Int. J. Biol. Macromol.*, 2025, **297**, 139704.
13 L. Z. Gao, J. Zhuang, L. Nie, J. B. Zhang, Y. Zhang, N. Gu, T. H. Wang, J. Feng, D. L. Yang, S. Perrett and X. Yan, *Nat. Nanotechnol.*, 2007, **2**, 577–583.
14 J. He, Y. Hou, Z. Zhang, J. Zhang, X. Yan, K. Fan and M. Liang, *Nano Biomed. Eng.*, 2024, **16**, 28–47.
15 W. P. Yang, X. Yang, L. J. Zhu, H. S. Chu, X. Y. Li and W. T. Xu, *Coord. Chem. Rev.*, 2021, **448**, 214170.
16 Z. Q. Zhuang, Y. N. Yu, S. P. Dong, X. L. Sun and L. Mao, *Anal. Bioanal. Chem.*, 2024, **416**, 5949–5964.
17 C. Liu, Y. M. Zhao, D. Xu, X. X. Zheng and Q. Huang, *Anal. Bioanal. Chem.*, 2021, **413**, 4013–4022.
18 I. Batool, A. Anwar, M. Imran and Z. I. Alvi, *Top. Catal.*, 2025, **68**, 823–855.

19 M. A. Ansari, S. Shoaib, W. Chauhan, R. M. Gahtani, U. Hani, M. N. Alomary, G. Alasiri, N. Ahmed, R. Jahan, N. Yusuf and N. Islam, *Environ. Res.*, 2024, **241**, 117522.
20 K. Y. Wu, Y. Feng, Y. S. Li, L. Li, R. Liu and L. D. Zhu, *Anal. Bioanal. Chem.*, 2020, **412**, 5477–5487.
21 Y. F. Chen, Y. Zhang, L. Jiao, H. Y. Yan, W. L. Gu and C. Z. Zhu, *Chin. J. Anal. Chem.*, 2021, **49**, 907–921.
22 L. L. Dugan, D. M. Turetsky, C. Du, D. Lobner, M. Wheeler, C. R. Almli, C. K. F. Shen, T. Y. Luh, D. W. Choi and T. S. Lin, *Proc. Natl. Acad. Sci. U. S. A.*, 1997, **94**, 9434–9439.
23 C. Zhao, J. Kang, Y. W. Li, Y. Wang, X. Y. Tang and Z. Q. Jiang, *Cyborg Bionic Syst.*, 2023, **4**, 0022.
24 Y. J. Song, K. G. Qu, C. Zhao, J. S. Ren and X. G. Qu, *Adv. Mater.*, 2010, **22**, 2206–2210.
25 H. Wang, P. H. Li, D. Q. Yu, Y. Zhang, Z. Z. Wang, C. Q. Liu, H. Qiu, Z. Liu, J. S. Ren and X. G. Qu, *Nano Lett.*, 2018, **18**, 3344–3351.
26 Z. Zhuang, Y. Yu, S. Dong, X. Sun and L. Mao, *Anal. Bioanal. Chem.*, 2024, **416**, 5949–5964.
27 X. Wan, Y. Ge, J. Zhang, W. Pan, N. Li and B. Tang, *ACS Appl. Mater. Interfaces*, 2023, **15**, 44763–44772.
28 L. Feng, L. Zhang, S. Zhang, X. Chen, P. Li, Y. Gao, S. Xie, A. Zhang and H. Wang, *ACS Appl. Mater. Interfaces*, 2020, **12**, 17547–17556.
29 J. Shen, J. Chen, Y. P. Qian, X. Q. Wang, D. S. Wang, H. G. Pan and Y. G. Wang, *Adv. Mater.*, 2024, **36**, 2313406.
30 E. Perez Mayoral, M. G. Ojer, M. Ventura and I. Matos, *Nanomaterials*, 2023, **13**, 2013.
31 X. M. Dang, H. G. Zhang, X. M. Chen and H. M. Zhao, *Sep. Purif. Technol.*, 2024, **330**, 125312.
32 Y. Qu, W. Zhang, B. Guang, Y. Xiao, X. Liu, C. Zhai and Y. Liu, *J. Alloys Compd.*, 2022, **912**, 165261.
33 Z. P. Lou, S. Zhao, Q. Wang and H. Wei, *Anal. Chem.*, 2019, **91**, 15267–15274.
34 H. Y. Yan, L. Z. Wang, Y. F. Chen, L. Jiao, Y. Wu, W. Q. Xu, W. L. Gu, W. Y. Song, D. Du and C. Z. Zhu, *Research*, 2020, **2020**, 8202584.
35 Y. Xiong, H. C. Li, C. W. Liu, L. R. Zheng, C. Liu, J. O. Wang, S. J. Liu, Y. H. Han, L. Gu, J. S. Qian and D. S. Wang, *Adv. Mater.*, 2022, **34**, 2110653.
36 Y. Y. Huang, C. Q. Liu, F. Pu, Z. Liu, J. S. Ren and X. G. Qu, *Chem. Commun.*, 2017, **53**, 3082–3085.
37 Y. F. Chen, L. Jiao, H. Y. Yan, W. Q. Xu, Y. Wu, H. J. Wang, W. L. Gu and C. Z. Zhu, *Anal. Chem.*, 2020, **92**, 13518–13524.
38 M. S. Kim, S. Cho, S. H. Joo, J. Lee, S. K. Kwak, M. I. Kim and J. Lee, *ACS Nano*, 2019, **13**, 4312–4321.
39 K. M. Tripathi, H. T. Ahn, M. Chung, X. A. Le, D. Saini, A. Bhati, S. K. Sonkar, M. I. Kim and T. Kim, *ACS Biomater. Sci. Eng.*, 2020, **6**, 5527–5537.
40 Y. Y. Gao, H. X. Li, Z. Z. Ou, P. Hao, Y. Li and G. Q. Yang, *Acta Phys.-Chim. Sin.*, 2011, **27**, 2469–2477.
41 X. Z. Chen, X. Y. Liu, S. F. Zhang, X. Y. Mu and X. D. Zhang, *Prog. Biochem. Biophys.*, 2023, **50**, 2684–2696.
42 X. Y. Xie, X. F. Chen, Y. H. Wang, M. S. Zhang, Y. X. Fan and X. P. Yang, *Talanta*, 2023, **257**, 124387.
43 Y. Xu, Y. J. Ma, X. H. Chen, K. Q. Wu, K. Y. Wang, Y. F. Shen, S. Q. Liu, X. J. J. Gao and Y. J. Zhang, *Angew. Chem., Int. Ed.*, 2024, **136**, 124387.
44 G. M. Li, H. Liu, T. D. Hu, F. Pu, J. S. Ren and X. G. Qu, *J. Am. Chem. Soc.*, 2023, **145**, 16835–16842.
45 W. W. Wu, L. Huang, X. Y. Zhu, J. X. Chen, D. Y. Chao, M. H. Li, S. L. Wu and S. J. Dong, *Chem. Sci.*, 2022, **13**, 4566–4572.
46 L. Jiao, J. B. Wu, H. Zhong, Y. Zhang, W. Q. Xu, Y. Wu, Y. F. Chen, H. Y. Yan, Q. H. Zhang, W. L. Gu, L. Gu, S. P. Beckman, L. Huang and C. Z. Zhu, *ACS Catal.*, 2020, **10**, 6422–6429.
47 L. Huang, J. X. Chen, L. F. Gan, J. Wang and S. J. Dong, *Sci. Adv.*, 2019, **5**, 5490.
48 Y. Wang, G. R. Jia, X. Q. Cui, X. Zhao, Q. H. Zhang, L. Gu, L. R. Zheng, L. H. Li, Q. Wu, D. J. Singh, D. Matsumura, T. Tsuji, Y. T. Cui, J. Zhao and W. T. Zheng, *Chem*, 2021, **7**, 436–449.
49 S. F. Ji, B. Jiang, H. G. Hao, Y. J. Chen, J. C. Dong, Y. Mao, Z. D. Zhang, R. Gao, W. X. Chen, R. F. Zhang, Q. Liang, H. J. Li, S. H. Liu, Y. Wang, Q. H. Zhang, L. Gu, D. M. Duan, M. M. Liang, D. S. Wang, X. Y. Yan and Y. D. Li, *Nat. Catal.*, 2021, **4**, 407–417.
50 Y. J. Chen, B. Jiang, H. G. Hao, H. J. Li, C. Y. Qiu, X. Liang, Q. Y. Qu, Z. D. Zhang, R. Gao, D. M. Duan, S. F. Ji, D. S. Wang and M. M. Liang, *Angew. Chem., Int. Ed.*, 2023, **62**, e202301879.
51 L. Jiao, Y. K. Kang, Y. F. Chen, N. N. Wu, Y. Wu, W. Q. Xu, X. Q. Wei, H. J. Wang, W. L. Gu, L. R. Zheng, W. Y. Song and C. Z. Zhu, *Nano Today*, 2021, **40**, 101261.
52 L. Jiao, W. Q. Xu, Y. Zhang, Y. Wu, W. L. Gu, X. X. Ge, B. B. Chen, C. Z. Zhu and S. J. Guo, *Nano Today*, 2020, **35**, 100971.
53 Q. M. Chen, Y. Liu, Y. W. Lu, Y. J. Hou, X. D. Zhang, W. B. Shi and Y. M. Huang, *J. Hazard. Mater.*, 2022, **422**, 126929.
54 H. J. Sun, Y. Zhou, J. S. Ren and X. G. Qu, *Angew. Chem., Int. Ed.*, 2018, **57**, 9224–9237.
55 N. Cheng, J. C. Li, D. Liu, Y. H. Lin and D. Du, *Small*, 2019, **15**, 1901485.
56 Y. Li, R. Javed, R. Li, Y. Y. Zhang, Z. Y. Lang, H. B. Zhao, X. Liu, H. M. Cao and D. X. Ye, *Food Chem.*, 2023, **406**, 135017.
57 Q. D. Zeng, H. H. Zhong, J. H. Liao, Q. Huo, B. P. Miao, L. Zeng, B. Zhang and G. H. Nie, *Biomater. Sci.*, 2024, **12**, 5150–5163.
58 S. F. Zhang, Y. H. Li, S. Sun, L. Liu, X. Y. Mu, S. H. Liu, M. L. Jiao, X. Z. Chen, K. Chen, H. Z. Ma, T. Li, X. Y. Liu, H. Wang, J. N. Zhang, J. Yang and X. D. Zhang, *Nat. Commun.*, 2022, **13**, 4744.
59 W. H. Gao, J. Y. He, L. Chen, X. Q. Meng, Y. N. Ma, L. L. Cheng, K. S. Tu, X. F. Gao, C. Liu, M. Z. Zhang, K. L. Fan, D. W. Pang and X. Y. Yan, *Nat. Commun.*, 2023, **14**, 160.
60 Y. Chong, Q. Liu and C. C. Ge, *Nano Today*, 2021, **37**, 101076.

61 H. J. Sun, A. D. Zhao, N. Gao, K. Li, J. S. Ren and X. G. Qu, *Angew. Chem., Int. Ed.*, 2015, **54**, 7176–7180.
62 X. H. Niu, Q. R. Shi, W. L. Zhu, D. Liu, H. Y. Tian, S. F. Fu, N. Cheng, S. Q. Li, J. N. Smith, D. Du and Y. H. Lin, *Biosens. Bioelectron.*, 2019, **142**, 111495.
63 M. C. Hu, Z. H. Yao and X. Q. Wang, *Abstr. Pap. Am. Chem. Soc.*, 2017, **254**, 3477–3502.
64 Y. F. Chen, L. Jiao, H. Y. Yan, W. Q. Xu, Y. Wu, L. R. Zheng, W. L. Gu and C. Z. Zhu, *Anal. Chem.*, 2021, **93**, 12353–12359.
65 C. Liu, W. B. Fan, W. X. Cheng, Y. P. Gu, Y. M. Chen, W. H. Zhou, X. F. Yu, M. H. Chen, M. R. Zhu, K. L. Fan and Q. Y. Luo, *Adv. Funct. Mater.*, 2023, **33**, 2213856.
66 M. F. Huo, L. Y. Wang, Y. W. Wang, Y. Chen and J. L. Shi, *ACS Nano*, 2019, **13**, 2643–2653.
67 H. Li, Q. Li, Q. Shi, Y. Wang, X. Liu, H. Tian, X. Wang, D. Yang and Y. Yang, *Food Chem.*, 2022, **389**, 132985.
68 J. J. X. Wu and H. Wei, *Prog. Chem.*, 2021, **33**, 42–51.
69 Y. Y. Qi, B. J. Li, D. D. Song, F. R. Xiu and X. Gao, *Spectrochim. Acta, Part A*, 2023, **297**, 122722.
70 Y. W. Wang, Q. Liu, L. X. Wang, S. R. Tang, H. H. Yang and H. B. Song, *Microchim. Acta*, 2019, **186**, 7.
71 P. K. Boruah and M. R. Das, *J. Hazard. Mater.*, 2020, **385**, 121516.
72 W. X. Zhang, M. Yang, H. Zhang, X. J. Yu, W. Zhang, A. T. S. Wee, X. Yan, J. W. Qi and J. S. Li, *Chem. Eng. J.*, 2022, **428**, 131080.
73 Q. M. Chen, Y. Liu, Y. W. Lu, Y. J. Hou, X. D. Zhang, W. B. Shi and Y. M. Huang, *J. Hazard. Mater.*, 2022, **422**, 126929.
74 X. F. Chen, Y. Wang, M. Feng, D. Deng, X. Y. Xie, C. X. Deng, K. N. Khattak and X. P. Yang, *Chin. Chem. Lett.*, 2023, **34**, 107969.
75 Q. L. Ma, X. Y. Zhang, R. N. Guo, H. X. Zhang, Q. F. Cheng, M. Z. Xie and X. W. Cheng, *Sep. Purif. Technol.*, 2019, **210**, 335–342.
76 Q. H. Feng, G. Wang, L. H. Xue, Y. S. Wang, M. L. Liu, J. Liu, S. T. Zhang and W. P. Hu, *ACS Appl. Nano Mater.*, 2023, **6**, 4844–4853.
77 C. Zhang, H. C. Li, C. Li and Z. Q. Li, *Molecules*, 2020, **25**, 168.
78 N. Y. Donkadokula, A. K. Kola, I. Naz and D. Saroj, *Rev. Environ. Sci. Bio/Technol.*, 2020, **19**, 543–560.
79 S. Varjani, P. Rakholiya, H. Y. Ng, S. M. You and J. A. Teixeira, *Bioresour. Technol.*, 2020, **314**, 123728.
80 X. F. Chen, Y. Wang, M. Feng, D. Deng, X. Y. Xie, C. X. Deng, K. N. Khattak and X. P. Yang, *Chin. Chem. Lett.*, 2023, **34**, 107969.
81 Q. H. Feng, G. Wang, L. H. Xue, Y. S. Wang, M. L. Liu, J. Liu, S. T. Zhang and W. P. Hu, *ACS Appl. Nano Mater.*, 2023, **6**, 4844–4853.
82 X. Y. Xie, Y. Zhao, Y. X. Fan, L. Jiang, W. Liu and X. P. Yang, *Langmuir*, 2024, **40**, 12671–12680.
83 J. Wang, J. J. Zhang, K. Y. Guo, Q. Y. Yue, K. X. Yin, X. Xu, Y. W. Li, Y. Gao and B. Y. Gao, *Adv. Funct. Mater.*, 2024, **34**, 2406790.
84 L. Jiao, W. Q. Xu, H. Y. Yan, Y. Wu, C. R. Liu, D. Du, Y. H. Lin and C. Z. Zhu, *Anal. Chem.*, 2019, **91**, 11994–11999.
85 Y. Wu, J. B. Wu, L. Jiao, W. Q. Xu, H. J. Wang, X. Q. Wei, W. L. Gu, G. X. Ren, N. A. Zhang, Q. H. Zhang, L. Huang, L. Gu and C. Z. Zhu, *Anal. Chem.*, 2020, **92**, 3373–3379.
86 X. H. Gao, J. J. Tang, H. R. Liu, L. B. Liu and Y. Z. Liu, *Drug Dev. Res.*, 2019, **80**, 438–445.
87 Y. W. Mao, J. Zhang, R. Zhang, J. Q. Li, A. J. Wang, X. C. Zhou and J. J. Feng, *Anal. Chem.*, 2023, **95**, 8640–8648.
88 W. Q. Xu, W. Y. Song, Y. K. Kang, L. Jiao, Y. Wu, Y. F. Chen, X. L. Cai, L. R. Zheng, W. L. Gu and C. Z. Zhu, *Anal. Chem.*, 2021, **93**, 12758–12766.
89 Y. J. Song, Y. Chen, L. Y. Feng, J. S. Ren and X. G. Qu, *Chem. Commun.*, 2011, **47**, 4436–4438.
90 W. J. Ma, J. J. Mao, X. T. Yang, C. Pan, W. X. Chen, M. Wang, P. Yu, L. Q. Mao and Y. D. Li, *Chem. Commun.*, 2019, **55**, 159–162.
91 F. F. Cao, L. Zhang, Y. W. You, L. R. Zheng, J. S. Ren and X. G. Qu, *Angew. Chem., Int. Ed.*, 2020, **59**, 5108–5115.
92 Y. J. Zhang, W. H. Gao, Y. A. Ma, L. L. Cheng, L. Zhang, Q. G. Liu, J. Y. Chen, Y. R. Zhao, K. S. Tu, M. Z. Zhang and C. Liu, *Nano Today*, 2023, **49**, 101768.
93 H. Zhou, J. Lu and X. L. Yin, *Biomaterials*, 2025, 123465.
94 Y. T. Su, F. Wu, Q. X. Song, M. J. Wu, M. Mohammadniaei, T. W. Zhang, B. L. Liu, S. S. Wu, M. Zhang, A. Li and J. Shen, *Biomaterials*, 2022, **281**, 121325.
95 P. Malla, Y. M. Wang and C. H. Su, *J. Nanobiotechnol.*, 2025, **23**, 130.
96 M. Sha, W. Q. Xu, Z. C. Wu, W. L. Gu and C. Z. Zhu, *Chem. J. Chin. Univ.s*, 2022, **43**, 1751–1756.
97 S. F. Cai, J. M. Liu, J. W. Ding, Z. Fu, H. L. Li, Y. L. Xiong, Z. Lian, R. Yang and C. Y. Chen, *Angew. Chem., Int. Ed.*, 2022, **61**, e202204502.
98 Y. Wang, Y. Y. Xu, J. Y. Song, X. T. Liu, S. J. Liu, N. Yang, L. Wang, Y. J. Liu, Y. W. Zhao, W. H. Zhou and Y. Y. Zhang, *Int. J. Nanomed.*, 2024, **19**, 5837–5858.
99 H. S. Han and K. Y. Choi, *Biomedicines*, 2021, **9**, 305.
100 M. F. Huo, L. Y. Wang, H. X. Zhang, L. L. Zhang, Y. Chen and J. L. Shi, *Small*, 2019, **15**, 1901834.
101 J. R. Zhu, Q. L. Li, X. Li, X. M. Wu, T. Yuan and Y. L. Yang, *Langmuir*, 2022, **38**, 6860–6870.
102 D. F. Cao, X. Y. Zhou, Q. Guo, M. Y. Xiang, M. H. Bao, B. S. He and X. Y. Mao, *Biomark. Res.*, 2024, **12**, 142.
103 L. Asaad, B. Pepperrell, E. McErlean and F. Furlong, *Int. J. Mol. Sci.*, 2025, **26**, 1274.
104 B. Riddhidev, K. Endri, L. Sabitri, N. K. Lauren, K. Nishanth, I. Dragan, H. P. M. Kay, S. James, T. William and T. L. M. Viranga, *Eur. J. Med. Chem.*, 2022, **244**, 114807.
105 Y. Sun, B. Xu, X. Pan, H. Wang, Q. Wu, S. Li, B. Jiang and H. Liu, *Coord. Chem. Rev.*, 2023, **475**, 214896.
106 Y. A. Ma, J. J. Zhao, L. L. Cheng, C. Li, X. J. Yan, Z. C. Deng, Y. J. Zhang, J. Liang, C. Liu and M. Z. Zhang, *Carbon*, 2023, **204**, 526–537.
107 J. Y. Lu, Y. L. Mao, S. P. Feng, X. Li, Y. K. Gao, Q. F. Zhao and S. L. Wang, *Acta Biomater.*, 2022, **148**, 310–322.
108 J. Shin, N. Y. Kang, B. Kim, H. Y. S. Hong, L. Yu, J. Kim, H. M. Kang and J. S. Kim, *Chem. Soc. Rev.*, 2023, **52**, 4488–4514.

109 P. Malla, Y. M. Wang and C. H. Su, *J. Nanobiotechnol.*, 2025, **23**, 7786–7824.
110 Y. Cai, Z. Xiao, T. Cheng, B. Yuan, Y. Cui, J. L. Chen, Y. Zhao, P.-T. Chou and Y.-K. Peng, *ACS Appl. Mater. Interfaces*, 2025, **17**, 37577–37585.
111 D. Q. Zhu, M. L. Zhang, C. Wang, P. P. Gai and F. Li, *Chem. Mater.*, 2022, **34**, 11072–11080.
112 S. H. Chen, S. W. Guan, J. Tan, W. Lu, H. F. Zhang, J. J. Qiu, H. Q. Zhu and X. Y. Liu, *Adv. Funct. Mater.*, 2024, **34**, 2411202.
113 Y. J. Ji, Y. Wang, H. Wang, J. S. Bai, J. S. Ren and X. G. Qu, *Angew. Chem., Int. Ed.*, 2025, e202505742.
114 H. Wei and E. K. Wang, *Chem. Soc. Rev.*, 2013, **42**, 6060–6093.
115 Y. H. Hu, X. J. J. Gao, Y. Y. Zhu, F. Muhammad, S. H. Tan, W. Cao, S. C. Lin, Z. Jin, X. F. Gao and H. Wei, *Chem. Mater.*, 2018, **30**, 6431–6439.
116 M. Q. Xu, W. W. Wang, H. Han, Y. P. Wei, J. Q. Sha and G. D. Liu, *Chem. Eng. J.*, 2023, **475**, 146324.
117 M. W. Liu, W. Q. Xu, Y. J. Tang, Y. Wu, W. L. Gu, D. Du, Y. H. Lin and C. Z. Zhu, *Angew. Chem., Int. Ed.*, 2025, **64**, e202424070.
118 R. Zhang, B. Jiang, K. Fan, L. Gao and X. Yan, *Nat. Rev. Bioeng.*, 2024, **2**, 849–868.
119 S. Khan, M. Sharifi, S. H. Bloukh, Z. Edis, R. Siddique and M. Falahati, *Talanta*, 2021, **224**, 121805.